

# Maximum precision charging of multi-qubit quantum batteries

Davide Rinaldi ,<sup>1</sup> Radim Filip ,<sup>2</sup> Dario Gerace ,<sup>1</sup> and Giacomo Guarneri ,<sup>1</sup>

<sup>1</sup>*Dipartimento di Fisica “A. Volta,” Università di Pavia, via Bassi 6, 27100 Pavia (Italy)*

<sup>2</sup>*Department of Optics and Quantum Optics Laboratory, Palacký University, 17. listopadu 12, 77146 Olomouc (Czech Republic)*

Precision, robustness, and efficiency are crucial aspects in the design of quantum technologies. Here, we show how genuine quantum features, together with non-Gaussianity, can be the key elements to achieve the best of these three aspects during a quantum battery-charging process. Taking inspiration from a light-matter interaction paradigm, i.e., the Jaynes-Cummings model, we employ the Full Counting Statistics to study the stochastic exchanges of energy between an entire stack of qubits and a single-mode electromagnetic field (or mechanical oscillator). Our study allows to conclude that charging the battery through a sequential protocol involving a quantum non-Gaussian field state guarantees extremely high-performances in the charging process, whose precision is maximized even under sub-optimal operating conditions. These results highlight the potential of non-Gaussian quantum state charging to achieve a robust quantum precision advantage over Gaussian states of the field by suppressing detrimental quantum fluctuations, thus making it suitable to ultimate tasks for which a significant degree of accuracy is required.

The role of energy in Physics is related to the capability of a system to actually perform work. An energy-based perspective can be profitably adopted to thoroughly study any quantum device, ranging from quantum information technologies [1–5] to thermal engines and refrigerators [6–13]. Recently, this particular point of view favoured the emergence of a field of research focused on the analysis of energy exchanges between quantum systems. The models developed within this field, in which energy plays a central role, are framed into the category of so-called quantum batteries [14–58]. Such models owe their definition [16] to their classification of energy exchanges into three main processes: energy injection, energy storage, and on-demand energy delivery, thus recalling the behaviour of everyday-life batteries. This field is presently on the spotlight [14, 15]: several theoretical works on quantum batteries, devoted to the exploration of the ultimate boundaries of quantum thermodynamics [28–39] as well as to the design of more and more efficient and noise-resilient devices [40–49], are accompanied by experimental realizations [50] on superconducting apparatuses [51–54], trapped-ion platforms [55], quantum dots [56], and nuclear-spin systems [57].

However, dealing with energy exchanges at a quantum level means that energy fluctuations cannot be neglected: their magnitude can assume values comparable to the average energy exchanges themselves. A simple (and yet effective) method to quantify energy fluctuations is the Full Counting Statistics [59–62], with which process-dependent thermodynamical quantities can be properly examined. Such technique can be employed, for instance, to quantify the charging process in a Jaynes-Cummings [63–66] quantum battery, i.e., a battery model consisting of a qubit (i.e., the battery) coupled to a single-mode electromagnetic field confined in a resonating cavity (i.e., the charger).

In this Letter, we leverage on the concepts and tools

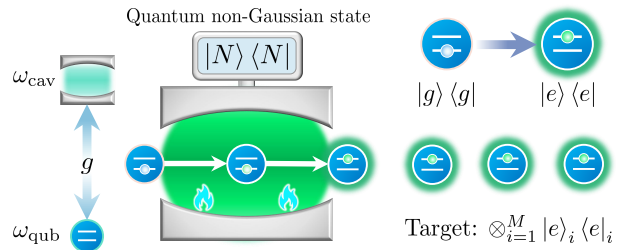


FIG. 1. Pictorial scheme of a multi-qubit JC quantum battery, where a precision advantage in the qubits charging can be obtained by exploiting a Fock state cavity. Under optimal model conditions (e.g., zero noise and perfect resonance), by coupling the cavity with a single qubit at a time, the entire stack of  $M$  qubits can be perfectly charged with a  $N$ -photon cavity Fock state, where  $N = M$ . Even in presence of noise or sub-optimal model parameters, a quantum non-Gaussian cavity state is still crucial to achieve an appreciable result.

of Quantum Thermodynamics to actually implement realistic quantum batteries with proven advantages in maximizing the charging precision. We specifically demonstrate that a multi-qubit quantum battery can be operated at an exceptionally low level of quantum fluctuations, crucial to envision a reliable quantum device, when a genuine quantum non-Gaussian state is employed as a charger. Such a quantum battery can then be employed to perform extremely fine precision tasks, such as quantum state preparation [67–69], or energy flow monitoring in quantum devices [70, 71].

*Introductory notes.* – The paradigmatic model for our proposal of quantum battery involves the prototypical Jaynes-Cummings (JC) interaction, which can be analytically solved [63–66]. Inspired by microwave cavity QED experiments [72], such model describes a qubit with resonance frequency  $\omega_{\text{qub}}$ , coupled to a single mode of an electromagnetic field confined to a cavity, characterized by

its harmonic oscillating frequency  $\omega_{\text{cav}}$ , as visualized in Fig. 1. The qubit-cavity coupling is determined by the interaction strength  $g$ , which here is assumed constant over time. In the broadly-available weak-coupling regime, in which  $g/\omega_0 \ll 1$ , with  $\omega_{\text{qub}} \simeq \omega_0 \simeq \omega_{\text{cav}}$ , the so-called counter-rotating terms in the Rabi Hamiltonian can be neglected by performing the rotating wave approximation (RWA) [63]. The JC Hamiltonian [63, 73–78] thus reads:

$$\hat{H}_{\text{JC}} = \hat{H}_{\text{free}} + \hbar g(\hat{\sigma}_+ \hat{a} + \hat{\sigma}_- \hat{a}^\dagger) \quad (1)$$

with  $\hat{H}_{\text{free}} = \hat{H}_{\text{qub}} + \hat{H}_{\text{cav}}$ ,  $\hat{H}_{\text{qub}} = \hbar \omega_{\text{qub}} \frac{1}{2} \hat{\sigma}_z$ , and  $\hat{H}_{\text{cav}} = \hbar \omega_{\text{cav}} \hat{a}^\dagger \hat{a}$ . The operator  $\hat{\sigma}_z$  is the  $z$ -Pauli matrix,  $\hat{\sigma}_-$  ( $\hat{\sigma}_+$ ) is the annihilation (creation) operator of a single qubit excitation, and  $\hat{a}$  ( $\hat{a}^\dagger$ ) is the annihilation (creation) operator of a single excitation in the single-mode field. The qubit state basis  $\{|e\rangle, |g\rangle\}$  consists of the pure excited state ( $|e\rangle$ ) and the pure ground state ( $|g\rangle$ ). In that basis, it is possible to define  $\hat{\sigma}_z = |e\rangle \langle e| - |g\rangle \langle g|$ ,  $\hat{\sigma}_- = |g\rangle \langle e|$ , and  $\hat{\sigma}_+ = |e\rangle \langle g|$ . We define the qubit state at time  $t$  as  $\hat{\rho}_{\text{qub}}(t)$ , and the cavity mode state as  $\hat{\rho}_{\text{cav}}(t)$ ; besides, at the initial time  $t = 0$ , the states of the two subsystems are assumed to be factorized:  $\hat{\rho}_{\text{JC}}(0) = \hat{\rho}_{\text{qub}}(0) \otimes \hat{\rho}_{\text{cav}}(0)$ . The cavity field state can be prepared [79] in an  $N$ -photon Fock state  $|N\rangle \langle N|$ , and, for a comparison, in a coherent state  $|\alpha\rangle \langle \alpha|$  with  $|\alpha\rangle = e^{-\frac{|\alpha|^2}{2}} \sum_{k=0}^{\infty} \frac{\alpha^k}{\sqrt{k!}} |k\rangle$  and  $|\alpha|^2$  photons on average, or in a quantum Gaussian state [80], such as a squeezed coherent state  $|\tilde{\alpha}, \zeta\rangle \langle \tilde{\alpha}, \zeta|$ , where  $\zeta$  is squeezing parameter.

The charging process consists of leading the qubit in its excited state, starting from its ground state, by exploiting the JC interaction. The goal is to achieve the maximum precision (i.e., lowest variance) possible on the energy exchanged between the cavity and the qubit during a time window  $\tau$ . To study the behaviour of such energy exchange, and thus characterizing its fluctuations over the duration of the interaction, we look at the stochastic variable [81]  $\Delta U_\tau$ . We define such variable ‘‘qubit internal energy’’, as it can be related to the measurement outcomes of a specific observable, i.e., the qubit Hamiltonian  $\hat{H}_{\text{qub}}$ , performed at two different times. The theoretical techniques developed to deal with it are encapsulated into the so-called Full Counting Statistics (FCS) [59]. Within FCS, the statistics of  $\Delta U_\tau$  is completely determined by a qubit-specific generating function  $\mathcal{G}_\tau(\chi)$ , such that  $\langle \Delta U_\tau^n \rangle = (-i)^n \frac{\partial^n \mathcal{G}(\chi)}{\partial \chi^n}|_{\chi=0}$ .  $\mathcal{G}_\tau(\chi)$  can be experimentally measured [82] and compared to the theoretically derived one when the underlying dynamical model is known. Indeed, the generating function can be computed as  $\mathcal{G}_\tau(\chi) = \text{Tr}\{\hat{\rho}_\chi(t)\}$ , where  $\hat{\rho}_\chi(t) = \hat{\mathcal{U}}_\frac{\chi}{2}(\tau, 0) \hat{\rho}_{\text{JC}}(0) \hat{\mathcal{U}}^\dagger_\frac{\chi}{2}(\tau, 0)$  and  $\hat{\mathcal{U}}_\frac{\chi}{2}(\tau, 0) = e^{i\frac{\chi}{2}\hat{H}_{\text{qub}}} \hat{\mathcal{U}}(\tau, 0) e^{-i\frac{\chi}{2}\hat{H}_{\text{qub}}}$  [59, 60]. The central figure of merit of our discussion is the signal-to-noise ratio (SNR),

which can be extracted from the statistics of  $\Delta U_\tau$ :

$$\text{SNR}(\Delta U_\tau) = \frac{\langle \Delta U_\tau \rangle^2}{\text{var}(\Delta U_\tau)} \quad (2)$$

being  $\text{var}(\Delta U_\tau) = \langle \Delta U_\tau^2 \rangle - \langle \Delta U_\tau \rangle^2$ . As it is evident from Eq. (2), the SNR quantifies how high the signal (i.e., the mean exchanged energy) is, compared to the magnitude of its fluctuation (i.e., its variance), and therefore constitutes the best measure of the process precision. Contextually, we use the fidelity  $F$  between the qubit state  $\hat{\rho}_{\text{qub}}(t)$  and the target state  $\hat{\rho}_{\text{target}} = |e\rangle \langle e|$ , defined as

$$F(t) = \text{Tr}\{[\hat{\rho}_{\text{qub}}^{\frac{1}{2}}(t) \hat{\rho}_{\text{target}} \hat{\rho}_{\text{qub}}^{\frac{1}{2}}(t)]^{\frac{1}{2}}\} \quad (3)$$

to quantify how likely the qubit can be driven in its excited state.

We now make the fundamental step to design a scalable implementation of a quantum battery, i.e., to investigate its capability of charging more than a single qubit with the maximal achievable precision. There are two possible way to accomplish this task: to charge the qubits (i) in a sequential manner, or (ii) in parallel, i.e., simultaneously.

*Sequential charging protocol.* – Let us assume to have a stack of  $M$  qubits, and that they can be coupled to the cavity one at a time via the following Hamiltonian:

$$\hat{H}_{\text{int}}(t) = \sum_{i=j}^M A_j(t) \hbar g(\hat{\sigma}_+^{(j)} \hat{a} + \hat{\sigma}_-^{(j)} \hat{a}^\dagger) \quad (4)$$

where  $A_j(t)$  is such that  $A_j(t) = 1$  if  $t \in [\tau_{j-1}, \tau_j]$ , and  $A_j(t) = 0$  otherwise. The  $j$ -th qubit interacts with the cavity during a time window  $\tau_j$  (in general,  $\tau_j \neq \tau_k$  for  $j \neq k$ , and for convenience  $\tau_0 \equiv 0$ ). After the interaction, the  $i$ -th qubit is immediately decoupled from the cavity, and at the same time the  $(j+1)$ -th qubit is coupled to the oscillator, analogously to the mechanism that occurs within a collisional-model description [83].

Due to the peculiarity of the model in Eq. (4), the Hamiltonians of different qubits commute between each other. Hence, we can apply the same formalism of a preparatory work [58], where the elementary case of a single qubit was discussed, to derive the SNR of the exchanged energy in a modular fashion, i.e., within each time window  $\tau_j$ . Importantly, we now keep track of the cavity state after each interaction. Such state, indeed, is never reset: the  $j$ -th charging round begins with the  $j$ -th qubit in a fresh ground state, while the cavity is set into the same state that it had at the end of the interaction with the  $(j-1)$ -th qubit.

As we show in Fig. 2, it is possible to perfectly charge  $M$  qubits by initializing the cavity in a  $N$ -photon Fock state with  $N = M$ , in principle. For that reason, the variance on the energy  $\Delta U_\tau$  injected in each qubit can be arbitrarily reduced to zero, provided that the interaction times  $\tau_i$  can be tuned with high precision. The

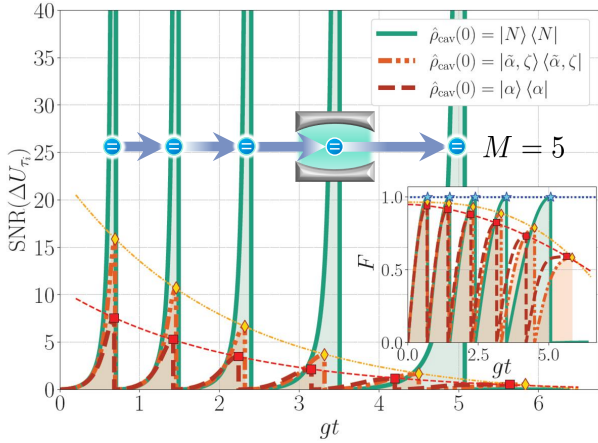


FIG. 2. Sequential charging of  $M = 5$  qubits, where  $\text{SNR}(\Delta U_{\tau_i})$  is calculated for each qubit charge. The fidelity  $F = F(t)$  between  $\hat{\rho}_{\text{qub}}^{(j)}(t)$  and  $\hat{\rho}_{\text{target}}^{(j)} = |e\rangle_j\langle e|_j$  is depicted in the inset. While the peaks associated with the Fock state SNR can be arbitrarily high, the ones related to the other states decrease exponentially in time. The fidelity can reach its maximum value  $F = 1$  only for the Fock state protocol; for the others, we always have  $F < 1$  and the peaks decrease in time as  $F \propto -(gt)^\gamma$ , with  $\gamma > 0$ . For that simulation, we used  $\langle n \rangle = N = 5$ ,  $\alpha = \sqrt{5}$  for the coherent state,  $\zeta = 0.6$  and  $\tilde{\alpha} \simeq 3.905$  for the squeezed coherent state, and  $g/\omega_{\text{qub}} = 10^{-2}$ . Here, we considered the resonant condition, i.e.,  $\Delta\omega = 0$ .

Fock state SNR therefore diverges, thus being arbitrarily higher than the SNR obtained via coherent or Gaussian states. The perfect charge of  $M$  qubits is confirmed by the fact that the fidelity between the  $j$ -th qubit states  $\hat{\rho}_{\text{qub}}^{(j)}(t)$  and  $\hat{\rho}_{\text{target}}^{(j)} = |e\rangle_j\langle e|_j$  can always reach  $F = 1$  for each charge round if the cavity is set in a Fock state. Furthermore, if the cavity is prepared in one of the other states, the maximum achievable fidelity per round is not only lower than 1, but it decreases after each interaction. As a final observation we note that, as expected, the time needed to charge the  $j$ -th qubit of the stack depends on the number of photons present in the cavity at the beginning of the charging process: in particular, for a  $N_j$ -photon Fock state cavity ready to charge the  $j$ -th qubit, the charging time  $\tau_j$  depends on  $N_j$  as  $\tau_j \propto 1/\sqrt{N_j}$  [17, 58].

*Parallel charging protocol.* – Next, we analyse the parallel charging protocol, for which we resort to the Tavis-Cummings (TC) model [84], which describes multiple mutually non-interacting qubits, each one simultaneously coupled to the single mode e.m. field confined to the cavity. The  $M$ -qubit TC Hamiltonian can be written as:

$$\hat{H}_{\text{TC}} = \hat{H}_{\text{free}} + \hbar g \sum_{j=1}^M (\hat{\sigma}_+^{(j)} \hat{a} + \hat{\sigma}_-^{(j)} \hat{a}^\dagger) \quad (5)$$

with  $\hat{H}_{\text{free}} = \hbar\omega_{\text{qub}} \sum_{j=1}^M \frac{\hat{\sigma}_z^{(j)}}{2} + \hbar\omega_{\text{cav}} \hat{a}^\dagger \hat{a}$ . Such model can be analytically solved for  $M \in \{1, \dots, 4\}$  qubits under

the perfect resonance condition, namely  $\Delta\omega = 0$  [84–86]. For what concerns our discussion, we study the case for  $M = 2$  analytically as a proof of concept, and solve numerically the cases for  $M \geq 3$ .

Here, we primarily considered the energy exchange of a single qubit, as well as the fidelity between the single qubit states  $\hat{\rho}_{\text{qub}}^{(j)}(t)$  and  $\hat{\rho}_{\text{target}}^{(j)} = |e\rangle_j\langle e|_j$ . Since the model is symmetric with respect to any permutation of the qubits, this is equivalent to study the fidelity between the  $M$ -qubit collective states  $\hat{\rho}_{\text{qub}}^{(1, \dots, M)}(t) = \bigotimes_{j=1}^M \hat{\rho}_{\text{qub}}^{(j)}(t)$  and  $\hat{\rho}_{\text{target}}^{(1, \dots, M)} = \bigotimes_{j=1}^M |e\rangle_j\langle e|_j$ .

The statistics related to the energetics of the single qubit can be derived by rotating the evolution operator as  $e^{i\frac{\chi}{2}\hat{O}}\hat{U}(\tau, 0)e^{-i\frac{\chi}{2}\hat{O}}$  with  $\hat{O} = \hat{H}_{\text{free}}^{\text{Q1}} = \hbar\omega_{\text{qub}} \frac{1}{2}\hat{\sigma}_z^{(1)}$ . In the specific  $M = 2$  case with  $\Delta\omega = 0$ , it is possible to demonstrate (see the Supplemental Material for the general proof) that, if  $\hat{\rho}_{\text{qub}}^{(1,2)}(0) = |g\rangle_1\langle g|_1 \otimes |g\rangle_2\langle g|_2$  and  $\hat{\rho}_{\text{cav}}(0) = |N\rangle\langle N|$ , then the SNR is quantified as:

$$\text{SNR}(\Delta U_{\tau}^{\text{Q1}}) = \frac{f(\tau, N) + h(\tau, N)}{1 - [f(\tau, N) + h(\tau, N)]} \quad (6)$$

being  $\omega_{\text{cav}} = \omega_0 = \omega_{\text{cav}}$ . The functions  $f(\tau, N)$  and  $h(\tau, N)$  are defined as:

$$f(\tau, N) \equiv \left[ \frac{-1 + \cos(g\tau\sqrt{2(2N-1)})}{2N-1} \right]^2 N(N-1) \quad (7)$$

$$h(\tau, N) \equiv \frac{\sin^2(g\tau\sqrt{2(2N-1)})}{2(2N-1)} N$$

Differences emerge if we consider the overall energy exchanged between cavity and qubits, which can be obtained by transforming the evolution operator with  $\hat{O} = \hbar\omega_{\text{qub}} \sum_{j=1}^M \frac{1}{2}\hat{\sigma}_z^{(j)}$  (with  $M = 2$  for the two-qubit case). In particular, the variance associated with the qubits ensemble is not directly proportional to the variances on the single-qubit energy (details can be found in the Supplemental Material).

On the numerical side, an effective way to numerically calculate the qubits energy statistics in the TC model is to solve a differential equation for the tilted density matrix  $\hat{\rho}_\chi(t)$  of the total system [60]:

$$\frac{d}{dt} \hat{\rho}_\chi(t) = -\frac{i}{\hbar} [\hat{H}_{\text{TC}, \chi} \hat{\rho}_\chi(t) - \hat{\rho}_\chi(t) \hat{H}_{\text{TC}, -\chi}] \quad (8)$$

where  $\hat{H}_{\text{TC}, \chi}$  is the tilted TC Hamiltonian  $\hat{H}_{\text{TC}, \chi} = \hat{H}_{\text{free}} + \hat{H}_{\text{int}, \chi}^{\text{Q1}}$ , being  $\hat{H}_{\text{int}, \chi}^{\text{Q1}}$  the  $M$ -qubit interaction Hamiltonian, transformed via the single-qubit free Hamiltonian:

$$\hat{H}_{\text{int}, \chi}^{\text{Q1}} = e^{i\frac{\chi}{2}\hat{H}_{\text{free}}^{\text{Q1}}} \hat{H}_{\text{int}} e^{-i\frac{\chi}{2}\hat{H}_{\text{free}}^{\text{Q1}}} \quad (9)$$

with  $\hat{H}_{\text{int}} = \hbar g \sum_{j=1}^M (\hat{\sigma}_+^{(j)} \hat{a} + \hat{\sigma}_-^{(j)} \hat{a}^\dagger)$ . Due to the absence of interactions between the qubits, it is possible to write

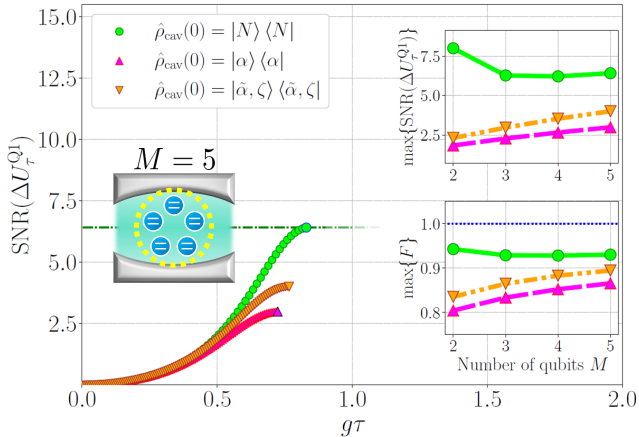


FIG. 3. SNR of the energy injected in a single qubit during the parallel charging of  $M = 5$  qubits, based on a numerical solution of the TC model. The upper inset shows the maximum SNR for  $M \in \{2, 3, 4, 5\}$  qubits, while the lower one depicts the maximum fidelity  $F$  between the state of the first qubit state  $\hat{\rho}_{\text{qub}}^{(1)}(1)$  and  $\hat{\rho}_{\text{target}}^{(1)} = |e\rangle_1 \langle e|_1$ , varying the number of qubits. From the insets, we observe that the SNR and the fidelity provided by the three different cavity states seem to approach each other in the high- $M$  limit. For that simulation, we used  $\langle n \rangle = N = 5$ ,  $\alpha = \sqrt{3}$  for the coherent state,  $\zeta = 0.6$  and  $\tilde{\alpha} \simeq 2.935$  for the squeezed coherent state,  $g/\omega_{\text{qub}} = 10^{-2}$ , and  $\Delta\omega = 0$ .

it as:

$$\begin{aligned} \hat{H}_{\text{int},\chi}^{(1)} = & \hbar g (\hat{\sigma}_+^{(1)} \hat{a} e^{i \frac{\chi}{2} \hbar \omega_{\text{qub}}} + \hat{\sigma}_-^{(1)} \hat{a}^\dagger e^{-i \frac{\chi}{2} \hbar \omega_{\text{qub}}}) \\ & + \hbar g \sum_{j=2}^M (\hat{\sigma}_+^{(j)} \hat{a} + \hat{\sigma}_-^{(j)} \hat{a}^\dagger) \end{aligned} \quad (10)$$

As reported in Fig. 3 for the parallel charging of  $M = 5$  qubits during a single time window  $\tau$ , the Fock state advantage in the SNR can not be arbitrarily enhanced by optimizing the model parameters, unlike the one related to the sequential charging protocol. As well, the charge of a single qubit can not be perfectly performed, since  $F < 1$  even for the Fock state protocol. Furthermore, it seems that the Fock state cavity performances get more and more comparable to the ones of the coherent and the Gaussian states on increasing  $M$ .

For these reasons, we conclude that the perfect charging of a stack of qubits with a single-mode field can be achieved only by employing a Fock state reservoir and a sequential protocol.

*Tolerance to noise.* – So far, we found that  $N$  qubits can be perfectly charged sequentially by using a  $N$ -photon Fock state cavity. However, it is reasonable to ask whether the qubits charging is robust even in presence of noise, thus determining the conditions under which the process precision is maximized. To address this issue, here we focus on the noise due to the presence of thermal photons, which can be detrimental to the quantum properties of the cavity state. Moreover, we discuss in the

Supplemental Material also the non-ideality introduced by other factors, such as errors in the cavity state preparation (or attenuation [87]), or a suboptimal choice for the model parameters.

We study the noise effects by simulating a sequential charging of  $M = 5$  qubits. For each charge of the entire stack of qubits, we set the mean number of initial photons  $\langle n \rangle$  in the cavity equal to a value among  $\{1, 2, 3, 4, 5\}$ . Then, we simulate the battery charge both when the cavity is initialized in a Fock state, and when it is prepared in a Gaussian state. We always consider the worst-case scenario: that is, we initialize the cavity in a noisy Fock state, but we compare its performances with an ideal (noiseless) Gaussian cavity state.

Given a certain parameter  $x$  (such as the number of thermal photons,  $\bar{n}_{\text{th}}$ ), we calculate the maximum SNR associated to the  $j$ -th qubit for a fixed  $\langle n \rangle$  over the charging time  $\tau_j$ , denoted as  $\max_{\tau_j} \{\text{SNR}_j(x, \langle n \rangle)\}$ , and we sum over  $j = 1, \dots, 5$ . Afterwards, we divide this sum by the mean number of initial photons  $\langle n \rangle$ , thus getting:

$$\overline{\text{SNR}}_{x,\langle n \rangle} \equiv \frac{1}{\langle n \rangle} \sum_{j=1}^5 \max_{\tau_j} \{\text{SNR}_j(x, \langle n \rangle)\} \quad (11)$$

In such way, the quantity defined in Eq. (11) represents an averaged SNR, normalized with respect to the field energy: this ensure the fairness of our findings, whose precision is no longer constrained by the resources (the initial number of photons) available to the experimenter. The figure of merit that we are going to use is then defined as the difference between the quantity (11) calculated for the Fock state cavity, and the one computed for the Gaussian state cavity:

$$D_{x,\langle n \rangle} = \overline{\text{SNR}}_{x,\langle n \rangle} \Big|_{\text{Fock}} - \overline{\text{SNR}}_{x,\langle n \rangle} \Big|_{\text{Gaussian}} \quad (12)$$

From the definition of  $D_{x,\langle n \rangle}$ , it is evident that a precision advantage of the Fock state over the Gaussian one corresponds to the condition  $D_{x,\langle n \rangle} > 0$ . Moreover,  $D_{x,\langle n \rangle}$  also accounts for situations where a cavity state with  $\langle n \rangle$  initial photons does not perfectly charge the first  $n$  qubits, but delivers the remaining energy to the subsequent ones.

To model the presence of thermal photons in the Fock state, we refer to Ref. [88], where a  $N$ -photon Fock state exposed to a source of additive thermal noise for a short period of time can be written in terms of the map  $\mathcal{K}$  such that:

$$\hat{\rho}_{\text{Fock}}^{\text{Th}} = \mathcal{K}(|N\rangle \langle N|) = \sum_{m=0}^{\infty} p_m(\bar{n}_{\text{th}}) |m\rangle \langle m| \quad (13)$$

This ‘thermalized’ Fock state is therefore a mixed state,

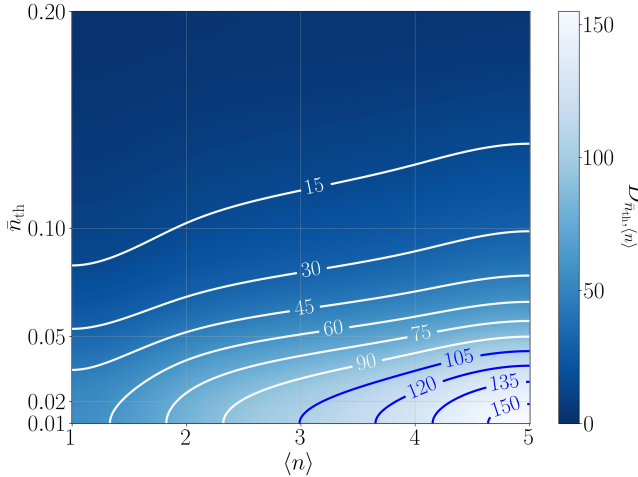


FIG. 4. Effect of the presence of  $\bar{n}_{\text{th}}$  thermal photons on average in a Fock state cavity. The sequential charging of 5 qubits has been simulated for each value of the initial number of photons in the cavity state,  $\langle n \rangle \in \{1, \dots, 5\}$ . The figure of merit is the difference  $D_{\bar{n}_{\text{th}}, \langle n \rangle}$  as defined in (12). Notice that  $D_{\bar{n}_{\text{th}}, \langle n \rangle}$  is always positive, meaning that the Fock state precision advantage is still persistent, even if affected by a low number of thermal photons. To compare with phase-insensitive Fock states, we used a Gaussian coherent squeezed state  $|\zeta, \tilde{\alpha}\rangle \langle \zeta, \tilde{\alpha}|$  with randomized phases [89] (for details, we refer to the Supplemental Material). For that simulation, as before, we used  $N = \langle n \rangle$  for the Fock state;  $\zeta$  and  $\tilde{\alpha}$  have been optimized to give the best performances for the squeezed coherent state. Besides,  $g/\omega_{\text{qub}} = 10^{-2}$ , and  $\Delta\omega = 0$ .

determined by the following probability distribution [88]:

$$p_m(\bar{n}_{\text{th}}, N) = \frac{m!}{N! \bar{n}_{\text{th}}} \sum_{k, k'=0}^m \frac{(-1)^{k+k'}}{k! k'!} \binom{N}{m-k} \times \binom{N}{m-k'} (k+k'+N-m)! \times \left(\frac{\bar{n}_{\text{th}}}{\bar{n}_{\text{th}}+1}\right)^{(k+k'+N-m+1)} \quad (14)$$

From Fig. 4, we observe that the difference  $D_{\bar{n}_{\text{th}}, \langle n \rangle}$  is positive even in presence of  $\bar{n}_{\text{th}} = 0.2$  on average; for lower values of  $\bar{n}_{\text{th}}$ , e.g., for  $\bar{n}_{\text{th}} = 0.02$ ,  $D_{\bar{n}_{\text{th}}, \langle n \rangle}$  can be considerably large (ranging from  $D_{\bar{n}_{\text{th}}, \langle n \rangle=1} \sim 50$  to  $D_{\bar{n}_{\text{th}}, \langle n \rangle=5} \sim 150$ ). Therefore, the precision advantage of the Fock state charging protocol seems to be robust against the presence of thermal noise, provided that the latter can be kept under a proper threshold. We also notice that the performances of the quantum non-Gaussian protocol increase with the mean number of photons  $\langle n \rangle$  that are initially present in the oscillator. In the end, the tolerance to the noise is larger the larger the initial number of photons  $N$  stored in the Fock state.

*Conclusions.* – In this manuscript we showed how a multi-qubit Jaynes-Cummings (JC) quantum battery

can be charged with the maximum possible precision by adopting a suitable charging protocol and by exploiting the properties of non-Gaussian quantum states. We compared two main ways to charge a stack of  $M$  qubits: sequentially and in parallel. We found that, under ideal conditions (i.e., in absence of noise), a  $N$ -photon Fock state cavity can perfectly charge exactly  $M = N$  qubits sequentially; on the other hand, the parallel charge, though faster, does not allow to achieve a perfect charge of the qubits.

Finally, we focused on the sequential protocol and tested its robustness under noise, by taking into account the presence of  $\bar{n}_{\text{th}}$  thermal photons on average. In spite of their detrimental effects, we observed that, within certain limits, a Fock state cavity increases the SNR by more than  $\sim 150$ , if compared to a cavity initialized in a Gaussian state, as can be evinced from Fig. 4. The maximum achievable precision can be therefore reached when a genuine quantum non-Gaussian state of the field is employed to charge the qubits in a sequential manner. This provides a reliable signature of the quantumness of the battery itself; moreover the latter, in principle, should be experimentally observable. Furthermore, our results apply also to recent experiments in circuit QED [90], trapped ions [91–93], and quantum electromechanics [94].

The analysis of imperfect cavity state preparation, of qubits with a nonzero excited-level population, and of nonzero detuning  $\Delta\omega$  between qubit and cavity is reported in the Supplemental Material, where we also discuss two model extensions of the single-qubit scenario: a time-dependent coupling strength  $J(t)$  in the JC model, and the presence of energy non-preserving operators in the JC Hamiltonian, namely the counter-rotating terms, that compose the Rabi Hamiltonian [95]. Details on the charging speed in the sequential and in the parallel charging protocols are also placed in the Supplemental Material.

Through the exploration of all these features, our proposal aims to provide a complete description that opens the way to a precise and efficient practical realization of a quantum battery.

*Acknowledgments.* – R.F. acknowledges the grant 21-13265X of the Czech Science Foundation. D.G. acknowledges the ‘National Quantum Science Technology Institute’ (NQSTI) within the PNRR project PE0000023. G.G. acknowledges funding from the Italian Ministry of Research (MUR) under the “Rita Levi Montalcini” project THESEUS. D.R. acknowledges A. Viola, E. Tumbiolo, G. Candreva, A. E. Mazzarone, L. Frau, D. Tona, G. Coppola, G. F. Conte, L. Marti, and R. G. Pozzi for the profound scientific discussions.

- 
- [1] S. Zaiser, T. Rendler, I. Jakobi, T. Wolf, S.-Y. Lee, S. Wagner, V. Bergholm, T. Schulte-Herbrüggen, P. Neumann, and J. Wrachtrup, *Nature communications* **7**, 12279 (2016).
- [2] C. L. Degen, F. Reinhard, and P. Cappellaro, *Reviews of modern physics* **89**, 035002 (2017).
- [3] J. Eisert, M. Wilkens, and M. Lewenstein, *Physical Review Letters* **83**, 3077–3080 (1999).
- [4] F. Arute, K. Arya, R. Babbush, D. Bacon, J. C. Bardin, R. Barends, R. Biswas, S. Boixo, F. G. Brandao, D. A. Buell, *et al.*, *Nature* **574**, 505 (2019).
- [5] T. D. Ladd, F. Jelezko, R. Laflamme, Y. Nakamura, C. Monroe, and J. L. O’Brien, *nature* **464**, 45 (2010).
- [6] J. P. Pekola, *Nature physics* **11**, 118 (2015).
- [7] J. Roßnagel, S. T. Dawkins, K. N. Tolazzi, O. Abah, E. Lutz, F. Schmidt-Kaler, and K. Singer, *Science* **352**, 325 (2016).
- [8] G. Maslennikov, S. Ding, R. Hablitzel, J. Gan, A. Roulet, S. Nimmrichter, J. Dai, V. Scarani, and D. Matsukevich, *Nature communications* **10**, 1 (2019).
- [9] D. Von Lindenfels, O. Gräß, C. T. Schmiegelow, V. Kaushal, J. Schulz, M. T. Mitchison, J. Goold, F. Schmidt-Kaler, and U. G. Poschinger, *Physical review letters* **123**, 080602 (2019).
- [10] J. Klaers, S. Faelt, A. Imamoglu, and E. Togan, *Physical Review X* **7**, 031044 (2017).
- [11] O. Onishchenko, G. Guarnieri, P. Rosillo-Rodes, D. Pijn, J. Hilder, U. G. Poschinger, M. Perarnau-Llobet, J. Eisert, and F. Schmidt-Kaler, *Nature Communications* **15** (2024), 10.1038/s41467-024-51263-3.
- [12] M. T. Mitchison, *Contemporary Physics* **60**, 164 (2019).
- [13] L. M. Cangemi, C. Bhadra, and A. Levy, *Physics Reports* **1087**, 1 (2024).
- [14] D. Ferraro, F. Cavaliere, M. G. Genoni, G. Benenti, and M. Sassetto, *Nature Reviews Physics* , 1 (2026).
- [15] F. Campaioli, S. Gherardini, J. Q. Quach, M. Polini, and G. M. Andolina, *Reviews of Modern Physics* **96**, 031001 (2024).
- [16] R. Alicki and M. Fannes, *Physical Review E—Statistical, Nonlinear, and Soft Matter Physics* **87**, 042123 (2013).
- [17] G. M. Andolina, D. Farina, A. Mari, V. Pellegrini, V. Giovannetti, and M. Polini, *Physical Review B* **98**, 205423 (2018).
- [18] F. Campaioli, F. A. Pollock, F. C. Binder, L. Céleri, J. Goold, S. Vinjanampathy, and K. Modi, *Phys. Rev. Lett.* **118**, 150601 (2017).
- [19] F. Barra, *Phys. Rev. Lett.* **122**, 210601 (2019).
- [20] F. Caravelli, G. Coulter-De Wit, L. P. García-Pintos, and A. Hamma, *Physical Review Research* **2**, 023095 (2020).
- [21] F. Tacchino, T. F. F. Santos, D. Gerace, M. Campisi, and M. F. Santos, *Phys. Rev. E* **102**, 062133 (2020).
- [22] V. Shaghaghi, V. Singh, M. Carrega, D. Rosa, and G. Benenti, *Entropy* **25**, 430 (2023).
- [23] D.-L. Yang, F.-M. Yang, and F.-Q. Dou, *Physical Review B* **109**, 235432 (2024).
- [24] A. Delmonte, A. Crescente, M. Carrega, D. Ferraro, and M. Sassetto, *Entropy* **23**, 612 (2021).
- [25] J. Carrasco, J. R. Maze, C. Hermann-Avigliano, and F. Barra, *Phys. Rev. E* **105**, 064119 (2022).
- [26] Z. Beleño, M. F. Santos, and F. Barra, *New Journal of Physics* **26**, 073049 (2024).
- [27] J.-Y. Gyhm and U. R. Fischer, *AVS Quantum Science* **6**, 012001 (2024).
- [28] S. Campbell, I. D’Amico, M. A. Ciampini, J. Anders, N. Ares, S. Artini, A. Auffèves, L. B. Oftelie, L. P. Bettmann, M. V. Bonançca, *et al.*, arXiv preprint arXiv:2504.20145 (2025).
- [29] D. Morrone, M. A. Rossi, and M. G. Genoni, *Physical Review Applied* **20**, 044073 (2023).
- [30] R. Grazi, D. Sacco Shaikh, M. Sassetto, N. Traverso Ziani, and D. Ferraro, *Physical Review Letters* **133**, 197001 (2024).
- [31] D. Morrone, *On the control of open quantum batteries*, Ph.D. thesis, Università degli Studi di Milano (2025).
- [32] I. Medina, O. Culhane, F. C. Binder, G. T. Landi, and J. Goold, *Physical Review Letters* **134**, 220402 (2025).
- [33] P. Sathe and F. Caravelli, *Europhysics Letters* **150**, 48001 (2025).
- [34] D. Murphy, A. Kiely, I. D’Amico, and S. Campbell, *Physical Review A* **112**, 052214 (2025).
- [35] G. M. Andolina, V. Stanzione, V. Giovannetti, and M. Polini, *Physical Review Letters* **134**, 240403 (2025).
- [36] G. M. Andolina, M. Keck, A. Mari, M. Campisi, V. Giovannetti, and M. Polini, *Physical review letters* **122**, 047702 (2019).
- [37] L. P. García-Pintos, A. Hamma, and A. Del Campo, *Physical Review Letters* **125**, 040601 (2020).
- [38] S. Tirone, R. Salvia, S. Chessa, and V. Giovannetti, *Physical Review Letters* **131**, 060402 (2023).
- [39] S. Tirone, R. Salvia, S. Chessa, and V. Giovannetti, *Physical Review A* **111**, 012204 (2025).
- [40] F. Cavaliere, G. Gemme, G. Benenti, D. Ferraro, and M. Sassetto, *Communications Physics* **8**, 76 (2025).
- [41] M. Hadipour, N. N. Yousefi, A. Mortezapour, A. S. Miavaghi, and S. Haseli, *Scientific Reports* **15**, 14578 (2025).
- [42] M.-L. Hu, T. Gao, and H. Fan, *Advanced Quantum Technologies* , e00422 (2025).
- [43] B. Polo and F. Centrone, arXiv preprint arXiv:2505.24604 (2025).
- [44] M. T. Mitchison, J. Goold, and J. Prior, *Quantum* **5**, 500 (2021).
- [45] B. Ahmadi, P. Mazurek, P. Horodecki, and S. Barzanjeh, *Physical Review Letters* **132**, 210402 (2024).
- [46] C. A. Downing and M. S. Ukhtary, *Physical Review A* **109**, 052206 (2024).
- [47] A. H. Malavazi, B. Ahmadi, P. Horodecki, and P. R. Dieguez, arXiv preprint arXiv:2510.25549 (2025).
- [48] R. Shastri, C. Jiang, G.-H. Xu, B. Prasanna Venkatesh, and G. Watanabe, *npj Quantum Information* **11**, 9 (2025).
- [49] A. Canzio, V. Cavina, M. Polini, and V. Giovannetti, *Physical Review A* **111**, 022222 (2025).
- [50] A. Camposeo, T. Virgili, F. Lombardi, G. Cerullo, D. Pisignano, and M. Polini, *Advanced Materials* **37**, 2415073 (2025).
- [51] C.-K. Hu, J. Qiu, P. J. Souza, J. Yuan, Y. Zhou, L. Zhang, J. Chu, X. Pan, L. Hu, J. Li, *et al.*, *Quantum Science and Technology* **7**, 045018 (2022).
- [52] S. N. Elyasi, M. A. Rossi, and M. G. Genoni, *Quantum Science and Technology* **10**, 025017 (2025).
- [53] S. Elghaayda, A. Ali, S. Al-Kuwari, A. Czerwinski, M. Mansour, and S. Haddadi, *Advanced Quantum Technologies* , 2400651 (2025).
- [54] L. Razzoli, G. Gemme, I. Khomchenko, M. Sassetto,

- H. Ouerdane, D. Ferraro, and G. Benenti, *Quantum Science and Technology* **10**, 015064 (2025).
- [55] J. Zhang, P. Wang, W. Chen, Z. Cai, M. Qiao, R. Li, Y. Huang, H. Tian, C. Luan, H. Tu, *et al.*, *Physical Review Letters* **135**, 140403 (2025).
- [56] I. Maillette de Buy Wenniger, S. Thomas, M. Maffei, S. Wein, M. Pont, N. Belabas, S. Prasad, A. Harouri, A. Lemaître, I. Sagnes, *et al.*, *Physical Review Letters* **131**, 260401 (2023).
- [57] J. Joshi and T. Mahesh, *Physical Review A* **106**, 042601 (2022).
- [58] D. Rinaldi, R. Filip, D. Gerace, and G. Guarnieri, *Physical Review A* **112**, 012205 (2025).
- [59] M. Esposito, U. Harbola, and S. Mukamel, *Reviews of Modern Physics* **81**, 1665 (2009).
- [60] G. T. Landi, D. Poletti, and G. Schaller, *Reviews of Modern Physics* **94**, 045006 (2022).
- [61] G. T. Landi, M. J. Kewming, M. T. Mitchison, and P. P. Potts, *PRX Quantum* **5**, 020201 (2024).
- [62] M. Brenes, G. Guarnieri, A. Purkayastha, J. Eisert, D. Segal, and G. Landi, *Physical Review B* **108**, L081119 (2023).
- [63] S. Stenholm, *Physics Reports* **6**, 1 (1973).
- [64] A. Smirne and B. Vacchini, *Physical Review A* **82**, 022110 (2010).
- [65] I. A. Bocanegra-Garay, L. Hernández-Sánchez, I. Ramos-Prieto, F. Soto-Eguibar, and H. M. Moya-Cessa, *SciPost Physics* **16**, 007 (2024).
- [66] J. Larson and T. Mavrogordatos, *The Jaynes–Cummings model and its descendants: modern research directions* (IoP Publishing, 2021).
- [67] D. Girolami, *Physical Review Letters* **122**, 010505 (2019).
- [68] E. A. Wollack, A. Y. Cleland, R. G. Gruenke, Z. Wang, P. Arrangoiz-Arriola, and A. H. Safavi-Naeini, *Nature* **604**, 463 (2022).
- [69] M. Kuzmanović, I. Björkman, J. J. McCord, S. Dogra, and G. S. Paraoanu, *Physical Review Research* **6**, 013188 (2024).
- [70] B.-L. Najera-Santos, P. A. Camati, V. Métillon, M. Brune, J.-M. Raimond, A. Auffèves, and I. Dotsenko, *Physical Review Research* **2**, 032025 (2020).
- [71] A. Franchi, D. Rossini, and E. Vicari, *Journal of Statistical Mechanics: Theory and Experiment* **2022**, 083103 (2022).
- [72] J.-M. Raimond, M. Brune, and S. Haroche, *Reviews of Modern Physics* **73**, 565 (2001).
- [73] A. Wallraff, D. I. Schuster, A. Blais, L. Frunzio, R. S. Huang, J. Majer, S. Kumar, S. M. Girvin, and R. J. Schoelkopf, *Nature* **431**, 162 (2004).
- [74] K. Hennessy, A. Badolato, M. Winger, D. Gerace, M. Atatüre, S. Gulde, S. Fält, E. L. Hu, and A. Imamoğlu, *Nature* **445**, 896 (2007).
- [75] S. De Liberato, D. Gerace, I. Carusotto, and C. Ciuti, *Phys. Rev. A* **80**, 053810 (2009).
- [76] D. Schuster, A. A. Houck, J. Schreier, A. Wallraff, J. Gambetta, A. Blais, L. Frunzio, J. Majer, B. Johnson, M. Devoret, *et al.*, *Nature* **445**, 515 (2007).
- [77] P. Forn-Díaz, L. Lamata, E. Rico, J. Kono, and E. Solano, *Reviews of Modern Physics* **91**, 025005 (2019).
- [78] F. Beaudoin, J. M. Gambetta, and A. Blais, *Physical Review A—Atomic, Molecular, and Optical Physics* **84**, 043832 (2011).
- [79] S. Deleglise, I. Dotsenko, C. Sayrin, J. Bernu, M. Brune, J.-M. Raimond, and S. Haroche, *Nature* **455**, 510 (2008).
- [80] G. Adesso, S. Ragy, and A. R. Lee, *Open Systems & Information Dynamics* **21**, 1440001 (2014).
- [81] J. M. Hickey, S. Genway, I. Lesanovsky, and J. P. Garrahan, *Physical Review B—Condensed Matter and Materials Physics* **87**, 184303 (2013).
- [82] J. Goold, U. Poschinger, and K. Modi, *Physical Review E* **90**, 020101 (2014).
- [83] F. Ciccarello, S. Lorenzo, V. Giovannetti, and G. M. Palma, *Physics Reports* **954**, 1 (2022).
- [84] K. Fujii, K. Higashida, R. Kato, and Y. Wada, *arXiv preprint quant-ph/0403008* (2004).
- [85] W. Lu, C. Zhai, H. Tao, Y. Song, J. Yuan, L. Xu, J. Tan, and S. Tang, *Physical Review A* **112**, 032441 (2025).
- [86] K. Fujii, K. Higashida, R. Kato, T. Suzuki, and Y. Wada, *International Journal of Geometric Methods in Modern Physics* **1**, 721 (2004).
- [87] U. Leonhardt, *Reports on Progress in Physics* **66**, 1207 (2003).
- [88] A. Ritboon, L. Slodička, and R. Filip, *Quantum Science and Technology* **7**, 015023 (2022).
- [89] A. Pradana and L. Y. Chew, *New Journal of Physics* **21**, 053027 (2019).
- [90] M. Hofheinz, E. Weig, M. Ansmann, R. C. Bialczak, E. Lucero, M. Neeley, A. O’Connell, H. Wang, J. M. Martinis, and A. Cleland, *Nature* **454**, 310 (2008).
- [91] C. Monroe, W. C. Campbell, L.-M. Duan, Z.-X. Gong, A. V. Gorshkov, P. W. Hess, R. Islam, K. Kim, N. M. Linke, G. Pagano, *et al.*, *Reviews of Modern Physics* **93**, 025001 (2021).
- [92] L. Podhora, L. Lachman, T. Pham, A. Lešundák, O. Číp, L. Slodička, and R. Filip, *Physical Review Letters* **129**, 013602 (2022).
- [93] L. Podhora, *Experimental quantum non-Gaussian mechanical states of a trapped ion*, Ph.D. thesis, Department of Optics, Faculty of Science, Palacký University (2024).
- [94] Q. R. Rahman, I. Kladarić, M.-E. Kern, L. Lachman, Y. Chu, R. Filip, and M. Fadel, *Physical Review Letters* **134**, 180801 (2025).
- [95] D. Braak, *Symmetry* **11**, 1259 (2019).

## Supplemental Material

### I. ANALYTICAL SOLUTION OF THE TWO-QUBIT TAVIS-CUMMINGS MODEL

The evolution operator  $\hat{U}_{\text{TC}}(\tau)$  of the  $M = 2$  Tavis-Cummings model can be written explicitly as a  $4 \times 4$  matrix of cavity operators. A detailed derivation can be found in [84, 85] (see in particular [85] for the terms  $a_{24} = a_{34}$  in the exponentiation of the interaction Hamiltonian) for the resonant case, i.e.,  $\omega_{\text{qub}} = \omega_{\text{cav}} = \omega_0$ . Here, we summarize the main results.

The evolution operator from time  $t = 0$  to time  $t = \tau$  can in general be written as:

$$\hat{U}_{\text{TC}}(\tau) = e^{-\frac{i}{\hbar} \hat{H}_{\text{TC}} \tau} = e^{-i \frac{\omega_0}{2} \hat{\sigma}_z^{(1)} \tau - i \frac{\omega_0}{2} \hat{\sigma}_z^{(2)} \tau - i \omega_0 \hat{a}^\dagger \hat{a} \tau} e^{-\frac{i}{\hbar} \hat{H}_{\text{int}} \tau} \quad (\text{S.1})$$

The tricky part of the computation consists of finding  $e^{-\frac{i}{\hbar} \hat{H}_{\text{int}} \tau}$ , which can be expressed as [84]:

$$e^{-\frac{i}{\hbar} \hat{H}_{\text{int}} \tau} = \begin{pmatrix} a_{11} & a_{12} & a_{13} & a_{14} \\ a_{21} & a_{22} & a_{23} & a_{24} \\ a_{31} & a_{32} & a_{33} & a_{34} \\ a_{41} & a_{42} & a_{43} & a_{44} \end{pmatrix} \quad (\text{S.2})$$

where the matrix elements  $a_{ij}$  are cavity operators defined by:

$$\begin{aligned} a_{11} &= \frac{\hat{N} + 2 + (\hat{N} + 1) \cos(g\tau \sqrt{2(2\hat{N} + 3)})}{2\hat{N} + 3} & a_{12} = a_{13} &= -i \frac{\sin(g\tau \sqrt{2(2\hat{N} + 3)})}{\sqrt{2(2\hat{N} + 3)}} \hat{a} \\ a_{14} &= \frac{-1 + \cos(g\tau \sqrt{2(2\hat{N} + 3)})}{2\hat{N} + 3} \hat{a}^2 & a_{21} = a_{31} &= -i \frac{\sin(g\tau \sqrt{2(2\hat{N} + 1)})}{\sqrt{2(2\hat{N} + 1)}} \hat{a}^\dagger \\ a_{22} = a_{33} &= \frac{+1 + \cos(g\tau \sqrt{2(2\hat{N} + 1)})}{2} & a_{23} = a_{32} &= \frac{-1 + \cos(g\tau \sqrt{2(2\hat{N} + 1)})}{2} \\ a_{24} = a_{34} &= -i \frac{\sin(g\tau \sqrt{2(2\hat{N} + 1)})}{\sqrt{2(2\hat{N} + 1)}} \hat{a} & a_{41} &= \frac{-1 + \cos(g\tau \sqrt{2(2\hat{N} - 1)})}{2\hat{N} - 1} (\hat{a}^\dagger)^2 \\ a_{42} = a_{43} &= -i \frac{\sin(g\tau \sqrt{2(2\hat{N} - 1)})}{\sqrt{2(2\hat{N} - 1)}} \hat{a}^\dagger & a_{44} &= \frac{\hat{N} - 1 + \hat{N} \cos(g\tau \sqrt{2(2\hat{N} - 1)})}{2\hat{N} - 1} \end{aligned} \quad (\text{S.3})$$

and  $\hat{N} = \hat{a}^\dagger \hat{a}$  represents the cavity number operator. Thus, by defining  $\hat{\sigma}_z = \begin{pmatrix} 1 & 0 \\ 0 & -1 \end{pmatrix}$ ,  $\hat{\sigma}_z^{(1)} = \hat{\sigma}_z \otimes \hat{\mathbb{I}}_2 \otimes \hat{\mathbb{I}}_{\text{cav}}$ , and  $\hat{\sigma}_z^{(2)} = \hat{\mathbb{I}}_1 \otimes \hat{\sigma}_z \otimes \hat{\mathbb{I}}_{\text{cav}}$  (being  $\hat{\mathbb{I}}_i$  and  $\hat{\mathbb{I}}_{\text{cav}}$  the identity operators on the  $i$ -th qubit Hilbert space and on the cavity Hilbert space, respectively), one can write:

$$\hat{U}_{\text{TC}}(\tau) = e^{-i\omega_0 \hat{N} \tau} \begin{pmatrix} a_{11} e^{-i\omega_0 \tau} & a_{12} e^{-i\omega_0 \tau} & a_{13} e^{-i\omega_0 \tau} & a_{14} e^{-i\omega_0 \tau} \\ a_{21} & a_{22} & a_{23} & a_{24} \\ a_{31} & a_{32} & a_{33} & a_{34} \\ a_{41} e^{+i\omega_0 \tau} & a_{42} e^{+i\omega_0 \tau} & a_{43} e^{+i\omega_0 \tau} & a_{44} e^{+i\omega_0 \tau} \end{pmatrix} \quad (\text{S.4})$$

### II. SINGLE-QUBIT AND TWO-QUBIT ENERGY STATISTICS IN THE TC MODEL

Given the explicit form of  $\hat{U}_{\text{TC}}(\tau)$ , we can exploit the FCS as in the preliminary work [58] to find an analytical expression for the statistics of the energy injected in a single qubit, as well as in both of them. To find the energy

statistics of the single qubit (for simplicity, we focus on the first qubit, denoted as Q1), we have to compute the tilted operator:

$$\hat{\mathcal{U}}_{\chi}^{\text{Q1}}(\tau) = e^{i\frac{\chi}{2}\frac{\hbar\omega_0}{2}\hat{\sigma}_z^{(1)}}\hat{\mathcal{U}}_{\text{TC}}(\tau)e^{-i\frac{\chi}{2}\frac{\hbar\omega_0}{2}\hat{\sigma}_z^{(1)}} \quad (\text{S.5})$$

$$\hat{\mathcal{U}}_{\chi}^{\text{Q1}}(\tau) = e^{-i\omega_0\hat{N}\tau} \begin{pmatrix} a_{11}e^{-i\omega_0\tau} & a_{12}e^{-i\omega_0\tau} & a_{13,\chi}e^{-i\omega_0\tau} & a_{14,\chi}e^{-i\omega_0\tau} \\ a_{21} & a_{22} & a_{23,\chi} & a_{24,\chi} \\ a_{31,-\chi}e^{+i\omega_0\tau} & a_{32,-\chi}e^{+i\omega_0\tau} & a_{33} & a_{34} \\ a_{41,-\chi}e^{+i\omega_0\tau} & a_{42,-\chi}e^{+i\omega_0\tau} & a_{43}e^{+i\omega_0\tau} & a_{44}e^{+i\omega_0\tau} \end{pmatrix} \quad (\text{S.6})$$

where  $a_{ij,\pm\chi} = a_{ij}e^{\pm i\frac{\chi}{2}\hbar\omega_0}$ . Analogously, the adjoint evolution operator modified with the parameter  $-\chi$  is:

$$\hat{\mathcal{U}}_{-\chi}^{\dagger \text{Q1}}(\tau) = \begin{pmatrix} a_{11}^{\dagger}e^{+i\omega_0\tau} & a_{21}^{\dagger} & a_{31,-\chi}^{\dagger} & a_{41,-\chi}^{\dagger}e^{-i\omega_0\tau} \\ a_{12}^{\dagger}e^{+i\omega_0\tau} & a_{22}^{\dagger} & a_{32,-\chi}^{\dagger} & a_{42,-\chi}^{\dagger}e^{-i\omega_0\tau} \\ a_{13,\chi}^{\dagger}e^{+i\omega_0\tau} & a_{23,\chi}^{\dagger} & a_{33}^{\dagger} & a_{43}^{\dagger}e^{-i\omega_0\tau} \\ a_{14,\chi}^{\dagger}e^{+i\omega_0\tau} & a_{24,\chi}^{\dagger} & a_{34}^{\dagger} & a_{44}^{\dagger}e^{-i\omega_0\tau} \end{pmatrix} e^{+i\omega_0\hat{N}\tau} \quad (\text{S.7})$$

being again  $a_{ij,\pm\chi}^{\dagger} = a_{ij}^{\dagger}e^{\pm i\frac{\chi}{2}\hbar\omega_0}$ . Now, if we assume that the qubits are initially prepared in the collective ground state  $|g\rangle_1\langle g|_1 \otimes |g\rangle_2\langle g|_2 \equiv |gg\rangle\langle gg|$  and that the initial cavity state is  $\hat{\rho}_{\text{cav}}(0)$ , we can compute the generating function associated with the statistics of the energy exchanged by the *first qubit only* as follows:

$$\begin{aligned} \mathcal{G}_1(\chi, \tau) &= \text{Tr}\{\hat{\mathcal{U}}_{\chi}^{\text{Q1}}(\tau)(|gg\rangle\langle gg| \otimes \hat{\rho}_{\text{cav}}(0))\hat{\mathcal{U}}_{-\chi}^{\dagger \text{Q1}}(\tau)\} \\ &= \text{Tr}\{a_{14}\hat{\rho}_{\text{cav}}(0)a_{14}^{\dagger}e^{i\chi\hbar\omega_0} + a_{24}\hat{\rho}_{\text{cav}}(0)a_{24}^{\dagger}e^{i\chi\hbar\omega_0} + a_{34}\hat{\rho}_{\text{cav}}(0)a_{34}^{\dagger} + a_{44}\hat{\rho}_{\text{cav}}(0)a_{44}^{\dagger}\} \end{aligned} \quad (\text{S.8})$$

By differentiating it with respect of  $\chi$ , we easily get the mean injected energy:

$$\langle \Delta U_{\tau}^{\text{Q1}} \rangle = (-i)\frac{\partial}{\partial \chi} \mathcal{G}_1(\chi) \Big|_{\chi=0} = \hbar\omega_0 \text{Tr}\{a_{14}\hat{\rho}_{\text{cav}}(0)a_{14}^{\dagger} + a_{24}\hat{\rho}_{\text{cav}}(0)a_{24}^{\dagger}\} \quad (\text{S.9})$$

and its variance:

$$\begin{aligned} \text{var}(\Delta U_{\tau}^{\text{Q1}}) &= (-i)^2 \frac{\partial^2}{\partial \chi^2} \mathcal{G}_1(\chi) \Big|_{\chi=0} - \langle \Delta U_{\tau}^{\text{Q1}} \rangle^2 \\ &= (\hbar\omega_0)^2 \text{Tr}\{a_{14}\hat{\rho}_{\text{cav}}(0)a_{14}^{\dagger} + a_{24}\hat{\rho}_{\text{cav}}(0)a_{24}^{\dagger}\} - \langle \Delta U_{\tau}^{\text{Q1}} \rangle^2 \end{aligned} \quad (\text{S.10})$$

If we use  $\hat{\rho}_{\text{qub}}(0) = |gg\rangle\langle gg|$  and  $\hat{\rho}_{\text{cav}}(0) = |N\rangle\langle N|$  as initial conditions, we obtain:

$$\begin{aligned} \langle \Delta U_{\tau}^{\text{Q1}} \rangle &= \hbar\omega_0 [f(\tau, N) + h(\tau, N)] \\ \text{var}(\Delta U_{\tau}^{\text{Q1}}) &= (\hbar\omega_0)^2 [f(\tau, N) + h(\tau, N)] - \langle \Delta U_{\tau}^{\text{Q1}} \rangle^2 \end{aligned} \quad (\text{S.11})$$

where the functions  $f(\tau, N)$  and  $h(\tau, N)$  are defined by:

$$\begin{aligned} f(\tau, N) &\equiv \text{Tr}\{a_{14}\hat{\rho}_{\text{cav}}(0)a_{14}^{\dagger}\} = \left[ \frac{-1 + \cos(g\tau\sqrt{2(2N-1)})}{2N-1} \right]^2 N(N-1) \\ h(\tau, N) &\equiv \text{Tr}\{a_{24}\hat{\rho}_{\text{cav}}(0)a_{24}^{\dagger}\} = \frac{\sin^2(g\tau\sqrt{2(2N-1)})}{2(2N-1)} N \end{aligned} \quad (\text{S.12})$$

as in the main text. The SNR is readily derived:

$$\text{SNR}(\Delta U_{\tau}^{\text{Q1}}) = \frac{f(\tau, N) + h(\tau, N)}{1 - [f(\tau, N) + h(\tau, N)]} \quad (\text{S.13})$$

Analogously, for what concerns the energy of the two qubits (labelled by Q1,Q2), we only have to compute the tilted operator by exponentiating the sum of the qubits free Hamiltonians:

$$\hat{\mathcal{U}}_{\chi}^{\text{Q1},\text{Q2}}(\tau) = e^{i\frac{\chi}{2}\frac{\hbar\omega_0}{2}(\hat{\sigma}_z^{(1)} + \hat{\sigma}_z^{(2)})}\hat{\mathcal{U}}_{\text{TC}}(\tau)e^{-i\frac{\chi}{2}\frac{\hbar\omega_0}{2}(\hat{\sigma}_z^{(1)} + \hat{\sigma}_z^{(2)})} \quad (\text{S.14})$$

This originates the following tilted operator:

$$\hat{\mathcal{U}}_{\chi}^{Q1,Q2}(\tau) = e^{-i\omega_0\hat{N}\tau} \begin{pmatrix} a_{11}e^{-i\omega_0\tau} & a_{12,\frac{\chi}{2}}e^{-i\omega_0\tau} & a_{13,\frac{\chi}{2}}e^{-i\omega_0\tau} & a_{14,\chi}e^{-i\omega_0\tau} \\ a_{21,-\frac{\chi}{2}} & a_{22} & a_{23} & a_{24,\frac{\chi}{2}} \\ a_{31,-\frac{\chi}{2}} & a_{32} & a_{33} & a_{34,\frac{\chi}{2}} \\ a_{41,-\chi}e^{+i\omega_0\tau} & a_{42,-\frac{\chi}{2}}e^{+i\omega_0\tau} & a_{43,-\frac{\chi}{2}}e^{+i\omega_0\tau} & a_{44}e^{+i\omega_0\tau} \end{pmatrix} \quad (\text{S.15})$$

as well as:

$$\hat{\mathcal{U}}_{-\chi}^{\dagger Q1,Q2}(\tau) = \begin{pmatrix} a_{11}^{\dagger}e^{+i\omega_0\tau} & a_{21,-\frac{\chi}{2}}^{\dagger} & a_{31,-\frac{\chi}{2}}^{\dagger} & a_{41,-\chi}^{\dagger}e^{-i\omega_0\tau} \\ a_{12,\frac{\chi}{2}}^{\dagger}e^{+i\omega_0\tau} & a_{22}^{\dagger} & a_{32}^{\dagger} & a_{42,-\frac{\chi}{2}}^{\dagger}e^{-i\omega_0\tau} \\ a_{13,\frac{\chi}{2}}^{\dagger}e^{+i\omega_0\tau} & a_{23}^{\dagger} & a_{33}^{\dagger} & a_{43,-\frac{\chi}{2}}^{\dagger}e^{-i\omega_0\tau} \\ a_{14,\chi}^{\dagger}e^{+i\omega_0\tau} & a_{24,\frac{\chi}{2}}^{\dagger} & a_{34,\frac{\chi}{2}}^{\dagger} & a_{44}^{\dagger}e^{-i\omega_0\tau} \end{pmatrix} e^{+i\omega_0\hat{N}\tau} \quad (\text{S.16})$$

where  $a_{ij,\pm\frac{\chi}{2}} = a_{ij}e^{\pm i\frac{\chi}{2}\hbar\omega_0}$  and  $a_{ij,\pm\chi} = a_{ij}e^{\pm i\chi\hbar\omega_0}$ . Again, by initializing the qubits in their ground state, the generating function related to the statistics of the energy exchanged by the *two qubits as a whole* turns out to be:

$$\begin{aligned} \mathcal{G}_{12}(\chi, \tau) &= \text{Tr}\{\hat{\mathcal{U}}_{\chi}^{Q1,Q2}(\tau)(|gg\rangle\langle gg| \otimes \hat{\rho}_{\text{cav}}(0))\hat{\mathcal{U}}_{-\chi}^{\dagger Q1,Q2}(\tau)\} \\ &= \text{Tr}\{a_{14}\hat{\rho}_{\text{cav}}(0)a_{14}^{\dagger}e^{i2\chi\hbar\omega_0} + a_{24}\hat{\rho}_{\text{cav}}(0)a_{24}^{\dagger}e^{i\chi\hbar\omega_0} + a_{34}\hat{\rho}_{\text{cav}}(0)a_{34}^{\dagger}e^{i\chi\hbar\omega_0} + a_{44}\hat{\rho}_{\text{cav}}(0)a_{44}^{\dagger}\} \end{aligned} \quad (\text{S.17})$$

As before, we straightforwardly find the energy statistics as:

$$\langle \Delta U_{\tau}^{Q1,Q2} \rangle = (-i) \frac{\partial}{\partial \chi} \mathcal{G}_{12}(\chi) \Big|_{\chi=0} = 2\hbar\omega_0 \text{Tr}\{a_{14}\hat{\rho}_{\text{cav}}(0)a_{14}^{\dagger}\} + \hbar\omega_0 \text{Tr}\{a_{24}\hat{\rho}_{\text{cav}}(0)a_{24}^{\dagger} + a_{34}\hat{\rho}_{\text{cav}}(0)a_{34}^{\dagger}\} \quad (\text{S.18})$$

and:

$$\begin{aligned} \text{var}(\Delta U_{\tau}^{Q1,Q2}) &= (-i)^2 \frac{\partial^2}{\partial \chi^2} \mathcal{G}_{12}(\chi) \Big|_{\chi=0} - \langle \Delta U_{\tau}^{Q1,Q2} \rangle^2 \\ &= 4(\hbar\omega_0)^2 \text{Tr}\{a_{14}\hat{\rho}_{\text{cav}}(0)a_{14}^{\dagger}\} + (\hbar\omega_0)^2 \text{Tr}\{a_{24}\hat{\rho}_{\text{cav}}(0)a_{24}^{\dagger} + a_{34}\hat{\rho}_{\text{cav}}(0)a_{34}^{\dagger}\} - \langle \Delta U_{\tau}^{Q1,Q2} \rangle^2 \end{aligned} \quad (\text{S.19})$$

We note that, as expected,  $\langle \Delta U_{\tau}^{Q1,Q2} \rangle = 2\langle \Delta U_{\tau}^{Q1} \rangle$ : indeed, since  $a_{24} = a_{34}$ , the last two terms in Eq. (S.18) sum up to  $2\hbar\omega_0 \text{Tr}\{a_{24}\hat{\rho}_{\text{cav}}(0)a_{24}^{\dagger}\}$ . On the other hand, the variances of the overall exchanged energy is not directly proportional to the one of the single qubit energy. This fact is reflected on the SNR of the two-qubit energy exchange: indeed, this reaches a peak before (and not in correspondence of) the SNR associated with the energy of the first qubit. This is evident from Fig. S.1, where the maximum of  $\text{SNR}(\Delta U_{\tau}^{Q1,Q2})$  does not coincide with the maximum of the single-qubit fidelity  $F$ .

To conclude this section, we note that the general  $M$ -qubit case can be approached numerically by solving Eq. (8) in the main text. More generally, we can write the tilted Hamiltonian as  $\hat{H}_{\text{TC},\chi} = \hat{H}_{\text{free}} + \hat{H}_{\text{int},\chi}^{Q1,\dots,QM}$ , where  $\hat{H}_{\text{int},\chi}^{Q1,\dots,QM}$  is the  $M$ -qubit interaction Hamiltonian, tilted with the total free  $M$ -qubit Hamiltonian, i.e.,

$$\hat{H}_{\text{int},\chi}^{Q1,\dots,QM} = e^{i\frac{\chi}{2}\hat{H}_{\text{free}}^{\text{qub}}} \hat{H}_{\text{int}} e^{-i\frac{\chi}{2}\hat{H}_{\text{free}}^{\text{qub}}} \quad (\text{S.20})$$

with  $\hat{H}_{\text{free}}^{\text{qub}} = \hbar\omega_{\text{qub}} \sum_{j=1}^M \frac{1}{2}\hat{\sigma}_z^{(j)}$ . Since the qubits do not interact between each other, such operator turns out to be:

$$\hat{H}_{\text{int},\chi}^{Q1,\dots,QM} = \hbar g \sum_{j=1}^M (\hat{\sigma}_+^{(j)} \hat{a} e^{i\frac{\chi}{2}\hbar\omega_{\text{qub}}} + \hat{\sigma}_-^{(j)} \hat{a}^{\dagger} e^{-i\frac{\chi}{2}\hbar\omega_{\text{qub}}}) \quad (\text{S.21})$$

The numerical integration of Eq. (8) with  $\hat{H}_{\text{TC},\chi} = \hat{H}_{\text{free}} + \hat{H}_{\text{int},\chi}^{Q1,\dots,QM}$  then allows us to compute the statistics of the  $M$ -qubit energy exchange  $\Delta U_{\tau}^{Q1,\dots,QM}$ .

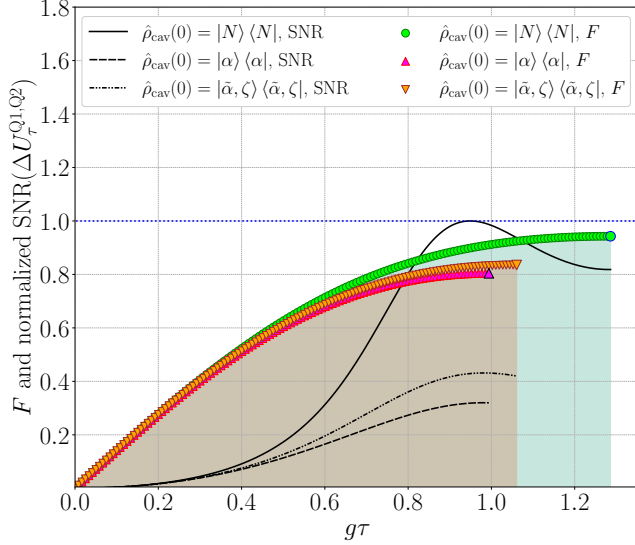


FIG. S.1. Fidelity  $F$  (discrete points) calculated for the single-qubit state, compared to the SNR of the two-qubits energy exchange  $\Delta U_{\tau}^{Q1,Q2}$ , normalized to its maximum value (black lines). As it can be observed, the maximum of the SNR does not occur in correspondence of the maximum of  $F$ : this means that the variance on the qubits collective energy is increased when the qubits are nearly charged. For that simulation, we used  $\langle n \rangle = N = 2$ ,  $\alpha = \sqrt{2}$  for the coherent state,  $\zeta = 0.6$  and  $\tilde{\alpha} \simeq 2.3$  for the squeezed coherent state, and  $g/\omega_{\text{qub}} = 10^{-2}$ . Here, we considered the perfect-resonance condition, i.e.,  $\Delta\omega = 0$ .

### III. ADDITIONAL NOISE ANALYSIS

Here, we complete the analysis of external factors that can diminish the Fock state advantage, ultimately corrupting the quantum features of the Fock state. One of these factors is the presence of state attenuation, which can be used to model imperfections in the cavity state preparation. Again, analogously to what we did to study the effects of thermal noise in the main text, we compare an attenuated Fock state of the field with a non-attenuated Gaussian state. Moreover, we also account for possible limitations due to a suboptimal choice of the model parameters: specifically, we consider off-resonance conditions (i.e., when  $\Delta\omega \neq 0$ ) and qubits which, instead of being prepared in their ground state, are initialized in low-temperature thermal states. In these two situations, both the Fock state and the Gaussian one are subject to the same choice of parameters.

#### A. State attenuation

Fock states are in general hard to be obtained: this implies that a realistic laboratory Fock state preparation can not be described by a pure state  $|N\rangle\langle N|$ . Rather, the prepared state will be a mixture of  $|N\rangle\langle N|$  with probability  $p$ , plus other terms like  $|N-k\rangle\langle N-k|$ , with  $k$  integer. We model this sort of linear “attenuation” acting on the Fock state as if the state  $|N\rangle\langle N|$  experienced some losses, which can be described by a beam splitter [87]. The resulting state is the one transmitted through the beam splitter with probability  $p$  (i.e., the square of the transmissivity  $t$ :  $p = t^2$ ), and its mathematical expression is therefore:

$$\hat{\rho}_{\text{Fock}}^{\text{Attenuated}} = \sum_{k=0}^N \binom{N}{k} p^k (1-p)^{N-k} |k\rangle\langle k| \quad (\text{S.22})$$

with  $\binom{N}{k} = \frac{N!}{k!(N-k)!}$ . From Fig. S.2 we can see that the difference  $D_{p,\langle n \rangle}$  is heavily affected by the presence of attenuation; however, for  $p \sim 0.95$ , the precision advantage is still considerable (for instance, see the case for  $p = 0.95$  and  $\langle n \rangle = 2$ :  $D_{p=0.95,\langle n \rangle=2} \simeq 25$ ). This is compatible with what has been experimentally observed in a trapped-ion device [93], where a Fock state  $|5\rangle$  can be prepared with probability  $p = 0.95$ .

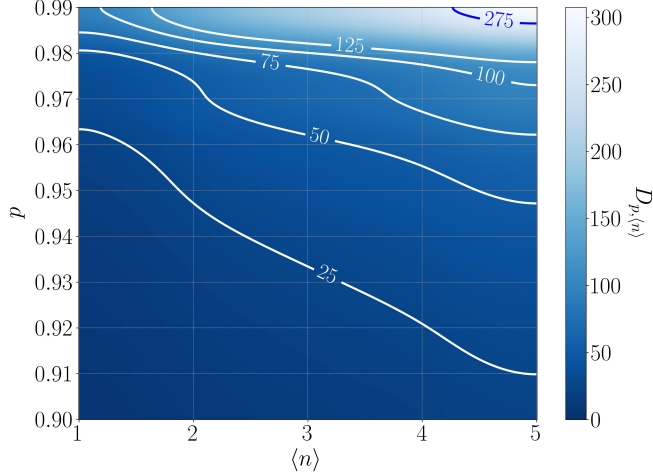


FIG. S.2. Effect of the cavity state attenuation, quantified by the probability  $p$  of preparing the Fock state  $|N\rangle\langle N|$ . If  $p = 1$ , the state is not attenuated at all, while if  $p = 0$  the state is completely suppressed. The figure of merit is now  $D_{p,\langle n \rangle}$ , thus depending on  $p$  and  $\langle n \rangle$ . Although the advantage quickly decreases as  $p < 1$ , there is still an appreciable difference  $D_{p,\langle n \rangle} \sim 25$  for  $p \simeq 0.95$ , which corresponds to the probability of preparing the Fock state  $|5\rangle$  in an ion trap [93] with current techniques. For that simulation, as for Fig. 4 in the main text, we used  $N = \langle n \rangle \in \{1, \dots, 5\}$  for the Fock state;  $\zeta$  and  $\tilde{\alpha}$  have been optimized to give the best performances for the squeezed coherent state. Besides,  $g/\omega_{\text{qub}} = 10^{-2}$ , and  $\Delta\omega = 0$ .

### B. Suboptimal parameter choices

We finally consider what happens to the charging performances if we vary the model parameters, thus missing the optimal conditions that allow for a perfect qubit charging. The first parameter that we change is the detuning  $\Delta\omega = \omega_{\text{qub}} - \omega_{\text{cav}}$  between qubit and cavity. The second one consists in the population  $q$  of the qubit excited level: we assume that the qubit is prepared in a low-temperature state defined as the mixture  $q|e\rangle\langle e| + (1-q)|g\rangle\langle g|$ . Fig. S.3 reports the results for both the parameters. Clearly, the presence of non-perfect resonance is not a problem for the battery performances: indeed, from Fig. S.3a it is possible to see that the difference  $D_{\Delta\omega,\langle n \rangle}$  is extremely high even for non-negligible detuning, such as  $\Delta\omega/\omega_{\text{qub}} = 10^{-3}$ . As an example, as reported in the figure, for  $\Delta\omega/\omega_{\text{qub}} = 10^{-3}$  and  $\langle n \rangle = 4$ , we get for instance  $D_{\Delta\omega,\langle n \rangle} \simeq 916$ . The true limiting factor, instead, is represented by the qubit populations  $q$ . Indeed, if we observe Fig. S.3b, we note that  $q \sim 0.01$  is sufficient to suppress the advantage down to  $D_{q,\langle n \rangle} \sim 30$  for  $\langle n \rangle = 1$ . Moreover,  $D_{q,\langle n \rangle}$  is further decreased as  $\langle n \rangle$  increases: this means that the presence of a populated excited state in the qubits also affects the charging of the overall stack of qubits.

## IV. CHARGING SPEED IN SEQUENTIAL AND PARALLEL PROTOCOLS

Another notable question regards the charging speed of a certain protocol, which is of interest in the study of quantum batteries. As can be noted by looking at Fig. 2 and Fig. 3 in the main text, the sequential charging protocol needs a longer time to be completed, if compared to the parallel one. This means that the first is slower than the second, and one may argue that this fact should be taken into account to define a genuine quantum advantage.

In that perspective, we made an ‘unfair’ comparison where a realistic (noisy) sequential protocol competes with an ideal (noiseless) parallel protocol to charge  $M = N$  qubits with a  $N$ -photon Fock state. In particular, for the sequential protocol, we choose some non-ideal initial conditions: the qubits are in a low-temperature thermal state with population  $q = 10^{-3}$ , and they are not in perfect resonance with the cavity:  $\Delta\omega/\omega_{\text{qub}} = 10^{-3}$ . Besides, only for the sequential protocol, we account for the presence of thermal photons (as an example, we choose  $\bar{n}_{\text{th}} = 10^{-2}$ ), as well as of attenuation (we choose  $p = 0.98$ ) in the initial cavity state.

To account for the charging speed, we thus define  $\tau_{\text{charge}}$  as the time needed to attain the maximum achievable charge in all the qubits. In the case of the parallel protocol,  $\tau_{\text{charge}}$  is simply the time that corresponds to the maximum SNR obtained in the single-qubit charging: therefore we use such maximum SNR divided by the dimensionless quantity

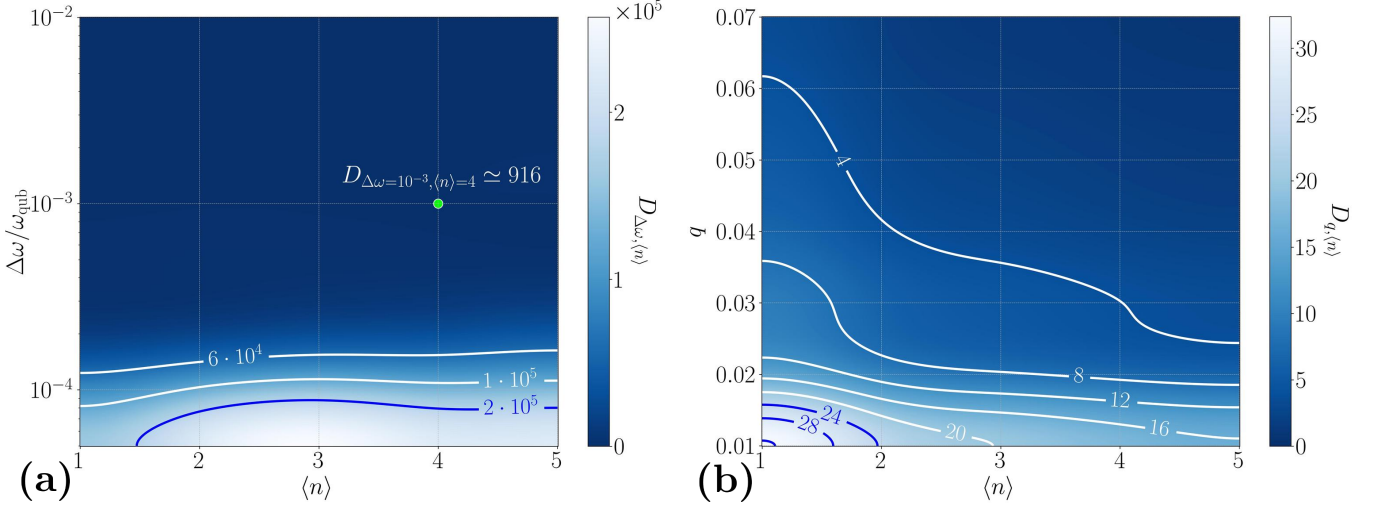


FIG. S.3. Effect of suboptimal choices of the model parameters, such as (a) the detuning  $\Delta\omega = \omega_{\text{qub}} - \omega_{\text{cav}}$  and (b) the qubit populations  $q$  such that  $\hat{\rho}_{\text{qub}}(\tau = 0) = q|e\rangle\langle e| + (1 - q)|g\rangle\langle g|$ . Note that, if  $q = 0$ , the qubit initial state is exactly the ground state  $|g\rangle\langle g|$ , while if  $q = 0.5$ , the qubit is in its maximally mixed state. The figures of merit are  $D_{\Delta\omega, \langle n \rangle}$  (dependent on  $\Delta\omega$  and  $\langle n \rangle$ ) for case (a), and  $D_{q, \langle n \rangle}$  (dependent on  $q$  and  $\langle n \rangle$ ) for case (b). The choice of the parameters is the same as in Fig. S.2. From (a), we can note that the Fock state advantage is very robust under the change of resonance conditions: indeed, non-negligible values of  $\Delta\omega/\omega_{\text{qub}}$  (such as  $\sim 10^{-3}$ ) allow for a conspicuous advantage. On the other hand, from (b) we see that the advantage is dramatically decreased in the case of non-zero qubit populations  $q$ . To maintain an appreciable advantage, thus, an experimental realization should assure the usage of low-temperature (nearly-ground state) qubits, for which at least  $q \lesssim 0.01$ . Besides, as the number of qubits increases, the advantage decreases in presence of a nonzero  $q$ , making this a considerable challenge to overcome when addressing the realization of a scalable quantum battery.

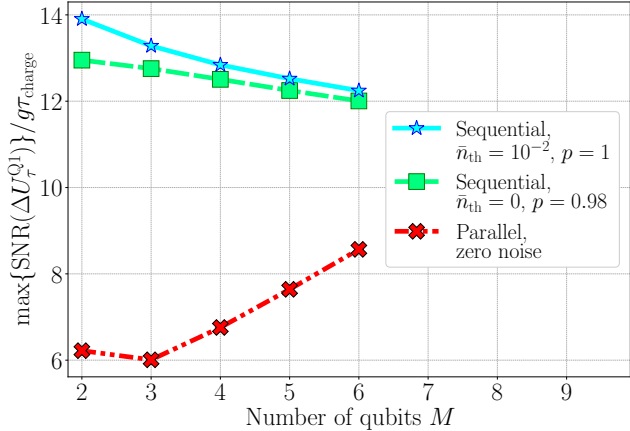


FIG. S.4. Worst-case comparison between realistic (noisy) sequential charging and ideal (noiseless) parallel charging of  $M = N$  qubits with a  $N$ -photon Fock state cavity. While the parallel protocol (red crosses) is simulated under perfect conditions (i.e., the qubits are in their ground state at the beginning of the protocol, they are perfectly resonant with the cavity, and no noise is present), the sequential one is performed with suboptimal model parameters and in presence of noise. In particular, for the latter we choose  $q = 10^{-3}$  and  $\Delta\omega/\omega_{\text{qub}} = 10^{-3}$ . The Figure displays the case with thermal noise but no attenuation ( $\bar{n}_{\text{th}} = 10^{-2}$  and  $p = 1$ , blue stars) and the case with attenuation but no thermal noise ( $\bar{n}_{\text{th}} = 0$  and  $p = 0.98$ , green squares). The points represent the average maximum SNR, divided by the time  $\tau_{\text{charge}}$  required to perform the charging of  $2 \leq M \leq 6$  qubits. The specific choice of parameters allows the realistic sequential protocol to achieve performances that are better than the parallel protocol. In spite of the fact that, for higher  $M$ , we expect the performances to be comparable to (if not worse than) the parallel charging, we point out that it is possible to arbitrarily increase the ones of the sequential charging by suppressing the noise and by choosing optimal model parameters.

$g\tau_{\text{charge}}$  as a figure of merit. In the case of the sequential protocol, instead,  $\tau_{\text{charge}}$  is the overall time needed to charge the entire chain of qubits, i.e., the time passed from the instant when the first qubit is coupled to the cavity, to the

instant when the last qubit is decoupled from it. We average the SNR achieved for each single-qubit charging by summing all the SNR maxima, and then we divide by the number of qubits that have been charged. We finally divide such averaged SNR by  $g\tau_{\text{charge}}$ .

From Fig. S.4 it is possible to see that the average SNR/time can be higher for the sequential protocol rather than the parallel one, at least for a small number of qubits. However, in the limit of a high number of qubits  $M$ , the parallel protocol seems destined to overcome the sequential one in terms of average SNR/time. This fact is reasonable, because the parallel protocol allows for achieving more or less the same SNR for each  $M$ , but the process takes shorter and shorter charging times  $\tau_{\text{charge}}$  as  $M$  increases. On the other hand, the sequential protocol allows to reach a higher SNR on average, but  $\tau_{\text{charge}}$  is longer as  $M$  is increased. Nevertheless, the average SNR/time in the sequential protocol can be arbitrarily enhanced by optimizing the model parameters and by suppressing the noise. Furthermore, we presented here a worst-case comparison: the parallel protocol, indeed, was simulated under ideal conditions. Even in that case, however, the sequential protocol proved itself to be capable of overcoming the parallel one at least for a finite number of qubits.

Moreover, it shows an expected no-free-lunch behaviour: using better resources, we can charge more precisely all qubits only if we go slower. On the other hand, if we want to speed up charging with much less precision, lower resources are sufficient.

## V. EXTENSIONS TO THE JAYNES-CUMMINGS MODEL

Now, we address the task of investigating models that are slightly more complicated than the Jaynes-Cummings paradigm. In particular, we first consider a time-dependent Jaynes-Cummings interaction, which makes the qubit-field coupling more realistic. Then, we account for the effects of additional terms in the Hamiltonian that appear in the Rabi model.

### A. Extension 1: Time-dependent interaction

As a first extension, we relax the hypothesis of constant coupling  $g$ . We thus consider a time-dependent JC model, where the time dependence is entirely encoded in a function  $J(t)$  that modulates the interaction Hamiltonian:

$$\hat{H}_{\text{int}}(t) = \hbar J(t)(\hat{\sigma}_+ \hat{a} + \hat{\sigma}_- \hat{a}^\dagger) \quad (\text{S.23})$$

This feature can be used to define more realistically the side effect of a finite-size cavity: we may think, for instance, of an e.m. field that is weaker near the cavity edges, but that is stronger and uniform near the center. We model such situation via a smoothed square function:

$$J(t) = \begin{cases} g[1 + e^{-(t-t_1^{(\delta)})/\delta}]^{-1} & \text{if } t < t_1^{(\delta)} + 10\delta \\ g & \text{if } t \in [t_1^{(\delta)} + 10\delta, t_2^{(\delta)} - 10\delta] \\ g[1 + e^{+(t-t_2^{(\delta)})/\delta}]^{-1} & \text{if } t > t_2^{(\delta)} - 10\delta \end{cases} \quad (\text{S.24})$$

where  $t_1^{(\delta)}, t_2^{(\delta)}$  are such that  $t_1^{(\delta)} = 20g\delta\tilde{t}$  and  $t_2^{(\delta)} = 2\tilde{t} - 20g\delta\tilde{t}$ , being  $\tilde{t}$  the time reference with respect to which the function  $J(t)$  is symmetric. In particular, we choose the parameters  $\tilde{t} = \tau_{\text{opt}}/2$  and  $\delta$  such that  $J(t=0) \simeq 0 \simeq J(t=\tau_{\text{opt}})$ , being  $\tau_{\text{opt}}$  the optimal time for which a perfect charging can be obtained by using a Fock state cavity with a constant coupling strength  $g$  [58]. As reported in Fig. S.5, a precision advantage of the Fock state cavity over the other states can still be obtained, and it can be arbitrarily enhanced as long as  $J(t)$  can approximate the constant value  $g$ , that is, when  $J(t) \simeq g$  for  $t \in [0, \tau_{\text{opt}}]$ , and  $J(t) = 0$  otherwise.

Since in the present situation the JC Hamiltonian is no longer time-independent, we can not use the analytical expression of the JC evolution operator  $\hat{U}_{\text{JC}}(t, 0)$  anymore. So, as before, we resort to a numerical solution of the differential equation for the tilted density matrix  $\hat{\rho}_\chi(t)$ , which reads [60]:

$$\frac{d}{dt} \hat{\rho}_\chi(t) = -\frac{i}{\hbar} [\hat{H}_{\text{JC},\chi}(t) \hat{\rho}_\chi(t) - \hat{\rho}_\chi(t) \hat{H}_{\text{JC},-\chi}(t)] \quad (\text{S.25})$$

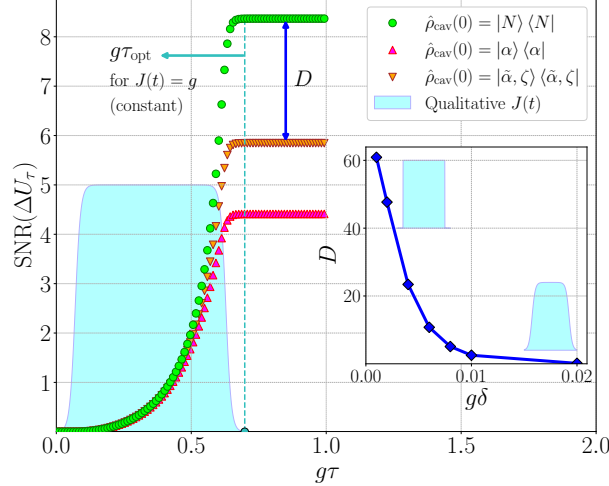


FIG. S.5. Example of non-uniform coupling strength  $J(t)$  over time. Here, we modelled  $J(t)$  as a smoothed square function (S.24) that is almost zero at the starting time  $\tau = 0$  and at the final time  $\tau_{\text{opt}}$ . As we can see, the advantage of the Fock state cavity over the other cavity states is still present, even if lowered if compared to the basic JC model case. The performances can be improved by approximating the coupling strength  $J(t) \simeq g \forall \tau \in [0, \tau_{\text{opt}}]$  as much as possible, as shown in the inset. Here, indeed, we can see that the difference  $D$  between the maximum SNR for the Fock state cavity and the one for the squeezed coherent state cavity increases as  $g\delta \rightarrow 0$ , so for a square-like  $J(t)$  (here,  $g/\omega_{\text{qub}} = 10^{-2}$  is maintained fixed, while  $\delta$  is varied). For that simulation, we used  $\langle n \rangle = N = 5$ ,  $\alpha = \sqrt{5}$  for the coherent state,  $\zeta = 0.6$  and  $\bar{\alpha} \simeq 3.905$  for the squeezed coherent state,  $g/\omega_{\text{qub}} = 10^{-2}$ , and  $\Delta\omega = 5 \cdot 10^{-3}$ . Besides, the parameters from Eq. (S.24) in the main plot have been chosen as  $g\delta = 10^{-2}$  and  $\tilde{t} = \tau_{\text{opt}}/2$ . In that way,  $t_1^{(\delta)} = 0.1\tau_{\text{opt}}$  and  $t_2^{(\delta)} = 0.8\tau_{\text{opt}}$ .

where  $\hat{H}_{\text{JC},\chi}(t)$  is the tilted JC Hamiltonian  $\hat{H}_{\text{JC},\chi}(t) = \hat{H}_{\text{free}} + \hat{H}_{\text{int},\chi}(t)$ , defined as:

$$\begin{aligned} \hat{H}_{\text{int},\chi}(t) &= e^{i\frac{\chi}{2}\hat{H}_{\text{qub}}}\hat{H}_{\text{int}}(t)e^{-i\frac{\chi}{2}\hat{H}_{\text{qub}}} \\ &= \hbar J(t)(\hat{\sigma}_+ \hat{a} e^{i\frac{\chi}{2}\hbar\omega_{\text{qub}}} + \hat{\sigma}_- \hat{a}^\dagger e^{-i\frac{\chi}{2}\hbar\omega_{\text{qub}}}) \end{aligned} \quad (\text{S.26})$$

and  $\hat{H}_{\text{free}} = \hat{H}_{\text{qub}} + \hat{H}_{\text{cav}}$ .

## B. Extension 2: Rabi model

The second model extension goes beyond the rotating-wave approximation (RWA): in that case, the JC paradigm changes its name into the Rabi model [95], whose Hamiltonian is:

$$\hat{H}_{\text{Rabi}} = \hbar\omega_{\text{qub}}\frac{\hat{\sigma}_z}{2} + \hbar\omega_{\text{cav}}\hat{a}^\dagger\hat{a} + \hbar g\hat{\sigma}_x(\hat{a} + \hat{a}^\dagger) \quad (\text{S.27})$$

Note that, for simplicity, we are restricting ourselves to the case of a constant coupling strength,  $J(t) = g$ . In the adopted qubit basis notation,  $\hat{\sigma}_x(\hat{a} + \hat{a}^\dagger)$  can be rewritten as  $\hat{\sigma}_+ \hat{a} + \hat{\sigma}_+ \hat{a}^\dagger \hat{\sigma}_- \hat{a} + \hat{\sigma}_- \hat{a}^\dagger$ . The counter-rotating terms (CRT) are the ones represented by  $\hat{\sigma}_+ \hat{a}^\dagger$  and  $\hat{\sigma}_- \hat{a}$ . As mentioned before, such terms are usually neglected in the weak-coupling regime via the RWA. These are not energy-preserving terms; however, if the model is written in interaction picture, they turn out to be weighted by complex phases as  $e^{\pm i(\omega_{\text{qub}} + \omega_{\text{cav}})t}$ , which mediate to zero as time flows (thus making the CRT vanishing), unless that  $g$  is comparable to  $\omega_{\text{qub}}$  and  $\omega_{\text{cav}}$ . In that case, these terms are no longer negligible and they should be taken into account.

The effects of the CRT are reported in Fig. S.6, which shows the numerical results obtained by finding the tilted evolution operator numerically. As expected, they can be limiting for the Fock state cavity advantage, since the maximum SNR does no longer diverge. However, it still largely outperforms the SNR computed for other cavity states. Nevertheless, we conclude that, in order to have a precision-focused quantum battery, the optimal regime in which to design the device is the JC one, i.e., the one for which qubit and cavity are weakly coupled, and thus the CRT can be safely neglected.

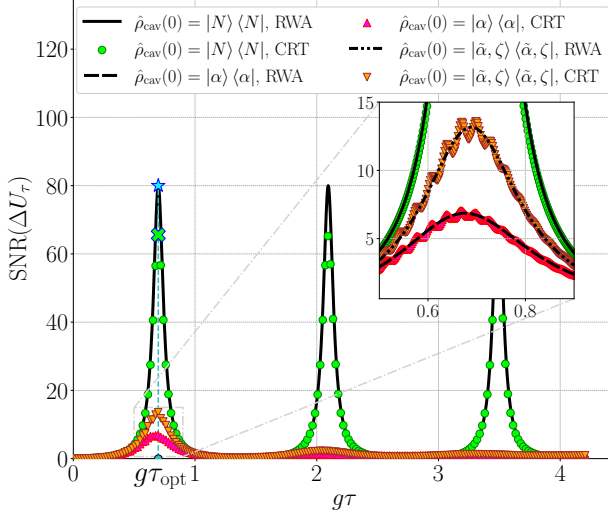


FIG. S.6. Inclusion of the counter-rotating terms (CRT)  $\hat{\sigma}_-\hat{a}$  and  $\hat{\sigma}_+\hat{a}^\dagger$  in the JC Hamiltonian. The quantum battery is now described by the Rabi model. The black lines represent the basic model, i.e., JC in rotating-wave approximation (RWA). The discrete points show the results for the Rabi model. Although when including the CRT the maximum of the Fock state SNR is lowered (green cross) with respect to the maximum in the RWA case (light blue star), a consistent advantage can still be observed. Besides, small oscillations in the SNR arise for the coherent and squeezed coherent states. For that simulation, we used  $\langle n \rangle = N = 5$ ,  $\alpha = \sqrt{5}$  for the coherent state,  $\zeta = 0.6$  and  $\tilde{\alpha} \simeq 3.905$  for the squeezed coherent state,  $g/\omega_{\text{qub}} = 10^{-2}$ , and  $\Delta\omega = 5 \cdot 10^{-3}$ .

## VI. PHASE RANDOMIZED STATE

To account for more realistic Gaussian states, we considered a phase-randomized coherent squeezed state [89] in place of the usual squeezed coherent state to perform the simulations related to the noise analysis. Such a state can be written as:

$$\hat{\rho} = \frac{1}{2\pi} \int_0^{2\pi} d\theta \sum_{n=0}^{\infty} \sum_{n'=0}^{\infty} p_n(\zeta, \tilde{\alpha}) p_{n'}(\zeta, \tilde{\alpha}) |n\rangle\langle n'| = \sum_{n=0}^{\infty} \mathcal{D}(n) |n\rangle\langle n| \quad (\text{S.28})$$

where the probability distribution over  $n$  is given by:

$$\mathcal{D}(n) = \frac{1}{n! \cosh r} \left[ \frac{1}{2} \tanh r \right]^n e^{-\left( |\alpha|^2 (1 + \tanh r) \right)} \left\{ H_n \left( |\alpha| \frac{1 + \tanh r}{\sqrt{2 \tanh r}} \right) \right\}^2 \quad (\text{S.29})$$

being  $H_n(x)$  the  $n$ -th Hermite polynomial of  $x$ , and  $r, \phi$  such that  $\zeta = r e^{i\phi}$ . The phase-randomized state (S.28) can be obtained from the explicit expression of the coherent squeezed state  $|\zeta, \alpha\rangle\langle\zeta, \alpha|$  (see [89] for details) such that:

$$|\zeta, \alpha\rangle = \sum_{n=0}^{\infty} \frac{1}{\sqrt{n! \cosh r}} \left[ \frac{1}{2} e^{i\phi} \tanh r \right]^{\frac{n}{2}} e^{-\frac{1}{2} \left( |\alpha|^2 + (\alpha^*)^2 e^{i\phi} \tanh r \right)} H_n \left( \frac{\alpha + \alpha^* e^{i\phi} \tanh r}{\sqrt{2 e^{i\phi} \tanh r}} \right) |n\rangle \equiv \sum_{n=0}^{\infty} p_n(\zeta, \alpha) |n\rangle \quad (\text{S.30})$$

by setting  $\phi = 2\theta$ , then integrating over  $\theta \in [0, 2\pi]$  and by dividing by  $2\pi$ .

We note that, when  $\alpha$  and  $\zeta$  are real numbers (and therefore  $\phi = 2m\pi$ , with  $m$  integer), then  $\mathcal{D}(n) = p_n^2$ : therefore, a Gaussian randomized-phase (diagonal) state and a Gaussian state with nonzero off-diagonal elements actually share the same diagonal elements. Because of that, this choice does not affect the performances of the Gaussian state if we consider diagonal qubits states of the form  $\hat{\rho}_{\text{qub}}(0) = q |e\rangle\langle e| + (1 - q) |g\rangle\langle g|$  at the beginning of the charging process. In that case, indeed, the qubit excited level population  $p_e(\tau)$  depends only on the diagonal elements of the initial cavity state,  $\hat{\rho}_{\text{cav}}(0)$ , which are the same in both cases. This can be easily demonstrated by looking at the JC evolution operator [58, 63–66], which we symbolically write here as  $\hat{U}_{\text{JC}}(\tau) = \begin{pmatrix} \hat{u}_{00} & \hat{u}_{01} \\ \hat{u}_{10} & \hat{u}_{11} \end{pmatrix}$ , where  $\hat{u}_{ij}$  are  $\tau$ -dependent cavity operators. Since the joint system evolved state is  $\hat{\rho}_{\text{JC}}(\tau) = \hat{U}_{\text{JC}}(\tau) \hat{\rho}_{\text{cav}}(0) \hat{U}_{\text{JC}}^\dagger(\tau)$ , we can write the excitation

probability  $p_e(\tau)$  as:

$$p_e(\tau) = \text{Tr}\{|e\rangle\langle e| \hat{\rho}_{\text{JC}}(\tau)\} = q\text{Tr}\{\hat{u}_{00}\hat{\rho}_{\text{cav}}(0)\hat{u}_{00}^\dagger\} + (1-q)\text{Tr}\{\hat{u}_{01}\hat{\rho}_{\text{cav}}(0)\hat{u}_{01}^\dagger\} \quad (\text{S.31})$$

We now may consider a non-diagonal cavity density matrix  $\hat{\rho}_{\text{cav}}(0) = \sum_{k,k'} \rho_{k,k'} |k\rangle\langle k'|$ . However, if we insert here the formulae for  $\hat{u}_{00}$  and  $\hat{u}_{01}$  (we refer to [58, 63–66] for their explicit expressions) into (S.31), we find:

$$p_e(\tau) = \sum_n q \cos^2(g\tau\sqrt{n+1})\rho_{n,n} + (1-q) \sin^2(g\tau\sqrt{n+1})\rho_{n+1,n+1} \quad (\text{S.32})$$

Thus, the only relevant matrix elements in  $\hat{\rho}_{\text{cav}}(0)$  are the diagonal ones, because  $p_e(\tau)$  depends only on them. Furthermore, since  $p_e(\tau)$  is intimately connected with the qubit energy, we conclude that also  $\langle\Delta U_\tau\rangle$  and  $\text{SNR}(\Delta U_\tau)$  do not change if we consider phase randomized cavity states in place of non-diagonal ones (provided that  $\alpha, \zeta \in \mathbb{R}$ , i.e., they are real numbers).